Nuclear Histone 3 Post-translational Modification Profiling in Whole Cells using Spectral Flow Cytometry

Histone H3 modification profiling using spectral flow

Carly S Golden[1*], Saylor Williams[1*], Sophia Blankevoort[2], Anna Belkina[1,3], H. Joseph Yost[4], Maria A Serrano[1‡]

[1]Center for Regenerative Medicine, Department of Medicine, Boston University Chobanian & Avedisian School of Medicine, Boston, USA

[2]John and Marcia Price College of Engineering, University of Utah

[3]Flow Cytometry Core Facility, Boston University Chobanian & Avedisian School of Medicine, Boston, USA

[4] The University of Utah, Salt Lake City, Utah and The Catholic University of America, Washington DC, USA

‡ For correspondence: maserr@bu.edu

*Contributed equally to this work

Abstract

Discerning the dynamic nature of nuclear histone 3 post-translational modifications (H3-PTMs) is crucial for understanding gene regulatory mechanisms. Although conventional nuclear H3-PTM flow cytometry protocols currently offer acceptable sensitivity, they typically involve isolating nuclei prior to running the assay, leading to significant sample loss and limited throughput. To address these challenges, we present a high-throughput nuclear H3-PTM spectral flow cytometry protocol conducted directly in whole cells. By performing fixation, permeabilization, and antibody incubations in a 96-well plate format, we eliminate the need for nuclei isolation, thereby preserving sample integrity and increasing throughput. Notably, this protocol allows for the simultaneous assessment of histone PTMs, cytoplasmic proteins, plasma membrane receptors, and cell cycle analysis within the same cell, providing comprehensive insights into the status and functional utility of a cell. This approach not only streamlines experimental procedures but also enhances the efficiency and reproducibility of nuclear flow cytometry assays, allowing for a deeper exploration of epigenetic regulation across diverse biological samples.

Summary Statement

We present a protocol for multi-parameter analysis of cell cycle, histone modifications, and caspase 3 in NPCs, utilizing spectral flow cytometry for improved sensitivity and sample integrity without nuclear enrichment.

Keywords: Spectral Flow Cytometry, Histone 3 post-translational modifications, Cell Cycle, Human induced pluripotent stem cells

Introduction

Cell cycle dynamics and histone modifications are critical in regulating lineage-specific gene expression during cell differentiation (Calder et al., 2013; Coronado et al., 2013; Hansen et al., 2008). Chromosome structure undergoes significant changes in histone modifications across various cell cycle phases during lineage commitment (Petruk et al., 2012). For instance, differentiating mitotic stem cells exhibit extended G1 phases as they exit pluripotency (Calder et al., 2013). Cell identity is established through progressive alterations in chromatin structure, driven by epigenetic mechanisms, including post-translational modifications (PTMs) of histones and lineage-specific transcription factors (Grigoryev et al., 2006; Larson and Yuan, 2012). Notably, H3 undergoes substantial PTM changes during germline induction (Weng et al., 2012). Recent work identifies a role of H3K27ac in bookmarking stem cell identity during mitosis, preserving essential histone PTMs and transcription factors (Yiyuan Liu et al., 2017). Therefore, to effectively identify regulatory mechanisms involved in lineage establishment, it is crucial to apply methods that can capture the dynamic changes in histone PTMs while resolving different cell cycle phases and cell identity marks.

Histone profiling via flow cytometry enables the study of global histone modification changes, providing detailed insights into chromatin dynamics at the single-cell level (Bergamasco et al., 2024; Ronzoni et al., 2005). However, traditional methods require isolating live cell nuclei and staining them in round-bottom tubes, which can lead to sample loss. Additionally, conventional flow cytometry uses a single detector per fluorophore, thus capturing only part of the emission spectrum, limiting multiplexing capabilities.

To overcome these limitations, we developed EpiFlow, an optimized whole-cell histone profiling protocol for spectral flow cytometry. EpiFlow utilizes a 96-well plate format for cell fixation, permeabilization, and staining, reducing reagent consumption and increasing throughput. Unlike most traditional histone PTM cytometry methods, our protocol does not require nuclear isolation, minimizing sample loss and enabling the detection of membrane-bound, cytoplasmic, and nuclear antigens. EpiFlow also leverages the multiplexing capability of spectral flow cytometry to increase the sensitivity of histone profiling while simultaneously collecting information from several cellular compartments and biological processes. Here, we present a validated spectral flow cytometry panel that identifies five histone PTMs typically associated with open chromatin alongside markers for cell cycle, apoptosis, and cell type identification in human induced pluripotent stem cells (hiPSC)-derived neuronal progenitor cells (NPC). To support the application, reproducibility, and improvement of EpiFlow and its analysis workflow, we created a GitHub repository (Golden et al., 2024; GitHub Repository) containing data and bioinformatic code written in a reproducible R environment (Ushey and Wickham, 2024a, 2024b), ensuring accessible and reproducible data analysis.

EpiFlow allows for the assessment of several histone PTMs and can resolve subtle changes across cell types and cell cycle phases in fixed samples. It offers higher resolution to explore relationships between histone PTMs, cell identity, and function, thus providing a useful tool to address complex biological questions. We propose that EpiFlow could inform, complement, and validate available next-generation sequencing approaches that examine chromatin biology.

Results and Discussion

Spectral flow cytometry employs more sensitive detectors that capture the full emission spectrum of each fluorochrome, permitting the use of larger panels to evaluate broader cell attributes (Ferrer-Font et al., 2021). Unique spectral signatures of each fluorochrome are identified through advanced unmixing techniques, addressing the compensation limitations observed in traditional flow (Novo, 2022). However, the limited availability of conjugated and validated monoclonal antibodies for histone PTMs represents a challenge for multiparametric panel design. To address this limitation during the design and validation of the EpiFlow panel, we selected histone PTM antibodies that met the following criteria: (a) availability of monoclonal antibodies conjugated with fluorochromes that have compatible spectral signatures for multiplexing, (b) histone marks with published literature supporting their association with transcriptional activation and distinct cell cycle phases; H3K27ac (Yin Liu et al., 2017; Yiyuan Liu et al., 2017), H3K4me3 (Lauberth et al., 2013), H3K9ac (Krejčí et al., 2009), H3K14ac (Kueh et al., 2023), H3K14ac+pH3 (Lo et al., 2000), H3K9ac+H3K14ac (Armenta-Castro et al., 2020; Karmodiya et al., 2012; Liu et al., 2023) and, (c) known responses to small molecules that will increase or decrease histone mark levels for validation purposes. This resulted in an initial histone H3 PTM core panel for H3K9ac, H3K14ac, H3K4me1, H3K4me3 and H3K27ac. Additional features to identify live/dead cells, total H3, distinct cell types, mitotic cells, apoptotic cells, and to resolve cell cycle phases were added based on spectral compatibility with the core H3-PTM panel (Supplementary Table 1). Our staining protocol was optimized to measure nuclear histone PTMs and features of interest across subcellular compartments in fixed whole cells. However, a significant challenge of this multiplexing approach is maintaining the integrity of membrane-bound epitopes while ensuring optimal fixation and permeabilization to allow antibodies sufficient access to the nuclear compartment and effective antigen recognition. To validate our staining protocol for cell membrane integrity and nuclear antigens accessibility, we performed immunofluorescence followed by confocal imaging of SCTi-003A hiPSCs stained with H3K9ac and beta-catenin (a membrane marker) (Fig. S1).

To assess the specificity of the selected antibodies, we treated SCTi-003A hiPSCs and WTC11 hiPSC-derived NPCs and with Trichostatin-A (TSA), SAHA (Vorinostat), or A-485 to selectively modulate histone H3 acetylation levels (Lasko et al., 2017; Richon et al., 1996; Seuter et al., 2013). TSA and SAHA are histone deacetylase I/II inhibitors (HDACi) that increase histone acetylation, while A485 is a histone acetyltransferase inhibitor (HATi) targeting the HAT coactivator complex p300/CBP, which ultimately reduces histone acetylation. We evaluated EpiFlow sensitivity using three different concentrations of these selective inhibitors and tested whether we could detect subtle changes in H3-PTMs across cell cycle phases. Our experiments in hiPSCs and NPCs showed a significant and dose-dependent change, either increasing (TSA and SAHA groups) or decreasing (A-485 group) median fluorescent intensity values (MFI) of H3K27ac, H3K4ac, and H3K9ac marks (Fig. S2, S3). Our results also showed distinct changes in the distribution of MFI values of each H3-PTM depending on both the expression levels of PAX6 (NPC marker) and cell cycle phase (Fig. S2 D, E). MFI is one of the most common statistics used to measure the shift in fluorescence intensity (FI) of a cell population. However, MFI values report the central tendency of a cell

114 population and do not provide information about the overall fluorescent distribution for a feature of interest
115 (Herzenberg et al., 2006; Roederer et al., 2004). This limitation is particularly relevant for experimental
116 designs aimed at detecting subtle changes in a feature's fluorescent profile, such as histone H3 acetylation
117 and methylation levels, as a response to drug treatments. TSA and A-485 are highly specific HDAC and
118 HAT inhibitors, respectively, widely used to modulate histone H3 acetylation levels (Lasko et al., 2017;
119 Vigushin et al., 2001). Therefore, we proposed that TSA and A-485 treatments would not change the FI
120 values of histone H3 methylation marks (H3K4me), further validating EpiFlow specificity. Interestingly,
121 H3K4me1 FI values showed significant differences between drug treatments and across cell cycle phases
122 (Krustal-Wallis test G0/G1 $\chi^2(6) = 4380.63$, $p<0.0001$; G2 $\chi^2(6) = 817.47$, $p<0.0001$; Mitosis $\chi^2(6) = 236.45$,
123 $p<0.0001$, Supplementary GitHub analysis, Methods Validation section). Further, the TSA group showed
124 an overall more pronounced effect on increased H3K4me1 signal than the A-485 group, particularly in
125 mitosis. Despite this, for all treatment groups, H3K4me1 MFI values shifted in the same direction towards
126 higher intensity values without affecting the overall signal distribution (Supplementary GitHub analysis,
127 Methods Validation section). We believe the observed H3K4me1 changes could indicate a technical
128 limitation of our approach or suggest an alternative scenario in which modulation of H3 acetylation might
129 also influence H3K4 methylation levels (Bui et al., 2010; Crump et al., 2011; Lee et al., 2006). This prompted
130 us to validate the sensitivity of our panel with two independent approaches: conventional flow cytometry to
131 measure H3K4 methylation levels in hiPSCs treated with either OICR-9429 or CPI-455 HCl, and in an
132 hiPSC line with a homozygous loss of function (LOF) mutation in the histone methyltransferase gene
133 *KMT2D* (KMT2D10.4). OICR-9429 is a potent antagonist that inhibits the WDR5-MLL complex responsible
134 for mediating H3K4me3, consequently reducing this mark (Grebien et al., 2015). CPI-455 HCL selectively
135 inhibits the lysine demethylase KDM5, resulting in increased global H3K4me3 levels (Vinogradova et al.,
136 2016). KMT2D10.4 hiPSCs were generated using a CRISPR/Cas9-targeted 2 base pair deletion in exon 2
137 of *KMT2D* gene in a WTC11 hiPSC line (File S1). The resulting line is expected to exhibit reduced levels of
138 H3K4 methylation compared to its isogenic control. WTC11 hiPSCs treated with OICR-9429 and CPI-455
139 HCL showed the expected shift in both the magnitude and direction of H3K4me3 FI (Fig. S4 C, E). This
140 was further supported by a significant reduction of H3K4me2 and H3K4me3 FI values in the *KMT2D* LOF
141 line compared to its isogenic control (Fig. S4 F). Although still significant, H3K4me1 levels remained
142 relatively consistent between the KMT2D10.4 and WTC11 cells (Fig. S4 A-C), which aligns with recent
143 studies reporting redundant H3K4me1 activity by other KMT2 methyltransferases in mouse embryonic stem
144 cells (Kubo et al., 2024). Our data, generated from three different hiPSC lines (SCTi-003A, WTC11, and
145 KMT2D10.4), in two cell types (hiPSC and NPC), acquired across two instruments (Aurora Cytek and
146 Stratedigm S1000EXi), demonstrate that EpiFlow can detect histone H3 PTMs with high sensitivity and
147 specificity. Additionally, our analysis underscores the importance of resolving the cell cycle status of cell
148 populations to identify histone PTM changes more accurately.

149 The simultaneous assessment of several cellular parameters in one experiment allows for high-
150 resolution profiling of complex samples, rare cell populations, or highly dynamic biological processes in

151 specific cell lineages. We hypothesized that EpiFlow could resolve distinct alterations of histone H3 PTM
152 across cell cycle phases in a single cell lineage, and that subtle variations in these modifications would
153 contribute to subcluster formation within each cell cycle phase. We again applied the core EpiFlow panel
154 (H3K4me3, H3K9ac, H3K27ac, H3K14ac and H3S10ph) to hiPSC-derived NPCs and included features that
155 identify live cells (Live/Dead staining), apoptotic cells (Cleaved-Caspase3), NPC (PAX6) and cell cycle
156 phases (FxCycle) (Table S1). All experiments were performed in triplicates (defined as one hiPSC line
157 cultured in three different wells followed by NPC induction) and included unstained cells and single-color
158 controls (SCCs) using beads or cells. After acquisition and unmixing (Detail in Supplementary File 2,
159 Supplementary File 3, and Analysis Note section), data was pre-processed following field standards to
160 remove low-quality events (Fig. 1, A-D) and enhance signal sensitivity and specificity (Supplementary File
161 3) (den Braanker et al., 2021; Herzenberg et al., 2006; Park et al., 2020). We used a traditional two-
162 dimensional gating strategy as a benchmark for a more exhaustive, unsupervised assessment and
163 exploratory analysis (Fig. 1 E-L). While downstream analysis used unsupervised algorithms, we defined
164 the minimum expected cluster resolution to inform the parameter selection and workflow. The criteria for
165 minimum expected clusters considered a relatively homogeneous cell population (NPC with varying levels
166 of PAX6 expression) captured at one of three possible stages of the cell cycle (based on markers used,
167 G0/G1, G2, or Mitosis (M)) or undergoing apoptosis (Cleaved-Caspase3). These clusters were expected to
168 have subtle differences in the levels of H3 PTM. Unlike traditional single-cell transcriptional data analysis,
169 unsupervised clustering of spectral flow data is performed in high-dimensional space, followed by
170 visualization in two-dimensional space. This approach optimizes the high-dimensional data captured by
171 EpiFlow while resolving subtle sub-populations (T et al., 2021). We used the clustering algorithm FlowSOM
172 (Van Gassen et al., 2015) followed by optimized t-stochastic neighbor embedding (opt-SNE) (Belkina et al.,
173 2019). Details about the parameters used in FlowSOM and opt-SNE can be found in Supplementary File
174 3. We first evaluated the quality of the FlowSOM clusters by comparing them with traditional gates in the
175 opt-SNE two-dimensional space (Fig. 2 A-C). To assess if the obtained clusters were consistent with
176 expected histone patterns (Li et al., 2005; Yiyuan Liu et al., 2017; Ma et al., 2015; Park et al., 2022; Pelham-
177 Webb et al., 2021; Sze et al., 2017; Van Rechem et al., 2021), we inspected the distribution and intensity
178 of each feature by plotting them in a color-continuous scale in the opt-SNE graphs (Fig. 2, D-L). Our analysis
179 resulted in 11 FlowSOM elbow metaclusters that, after careful exploration of all features, were consolidated
180 into 10 clusters (Fig. 2, C; fsom clusters 01-10. For details on merged clusters, see Supplementary File 3).
181 Unsupervised clustering resolved the expected cell populations (Fig.2 D-G) and identified unique cell states
182 or clusters that could potentially be driven by distinct H3 PTM patterns (Fig. 2 C, H-L).

183 Visualization of clusters and features in a two-dimensional space can be useful for initial feature
184 exploration of spectral flow cytometry data. However, the axis and global distances in these plots are
185 meaningless and can be affected by data distortion reported in transcriptional data analysis (Chari and
186 Pachter, 2023; T et al., 2021). Therefore, two-dimensional representations will not accurately reflect the
187 relationships between data points in high-dimensional space. To confirm that each identified cluster

represents a distinct and biologically meaningful group of cells, rather than being clustered together by random chance, we analyzed the contribution of H3 PTM patterns in each cluster to determine whether they reliably reflect the cell state or identity. In Figure 3, we evaluated the relative contribution of all features to each cluster, examined the distribution of FI values for all H3 PTMs within each cluster, and analyzed the correlation between features and clusters. In this article, we highlight clusters fsom_08 and fsom_09 as examples. These clusters had similar levels of PAX6 expression (known NPC) and DNA content (FxCycle denoting cells in G2) with subtle differences in FI values for H3 PTMs. Cluster 10 is also discussed due to its unique signature across all features (PAX6 and phH3_S10 double positive cells representing mitotic NPC) (Fig. 3). For a full analysis of all clusters, refer to the associated GitHub Repository. Our analysis showed that NPCs in clusters 08 and 09 shared the same five leading features (FxCycle, PAX6, H3K4me3, H3K9ac, and H3K27ac), but PAX6 and H3K27ac contributed differently to each cluster (Fig. 3 A, B). Additionally, while H3K9ac contributed relatively similarly to both clusters (Fig. 3 A, B; third bar), its FI distribution varied between them (Fig. 3 C, E). Our statistical analysis revealed significant differences in the FI and distribution of H3K4me3, H3K9ac, H3K14ac, and H3K27ac across the clusters, suggesting their potential role in distinguishing the biological state of the cells within each cluster (Fig. 3, G-J, Dunn pairwise test for selected clusters. Fig. S5, Krustal-Wallis test for all clusters). When H3 PTMs and cell cycle features are assessed across each cluster, we observed significant differences, suggesting that these clusters represent distinct cellular states of NPCs with varying FI distributions for the analyzed features (Fig. S6).

Our work demonstrates that EpiFlow can effectively resolve subtle patterns of histone H3 PTM across cell cycle phases with high resolution. With careful panel design, EpiFlow has the potential to explore the relationship between histone PTMs, transcription factors, and lineage commitment in varying cell types and samples, including cell cultures, organoids, and biopsies. Moreover, through the associated GitHub repository, we provide a reproducible and accessible workflow for the exploratory and statistical analysis presented in this article. With this work, we hope to facilitate the application of EpiFlow and its data analysis.

Limitations of this study

While EpiFlow can detect subtle differences within fairly homogenous cell populations, assigning labels or identities to clusters is limited by the markers used in the panel, such as PAX6 or DNA content for cell cycle phases. Furthermore, EpiFlow does not provide genomic information about the histone marks nor link these modifications to specific chromatin regions or regulatory elements. Therefore, inferring the biological relevance of a given cluster based on its H3-PTM profile is not possible without downstream analyses and validation.

Technical notes

Panel design and optimization are two of the most critical steps in spectral flow cytometry experiments, as they ensure sensitivity and reproducibility of results. Below, we provide general guidelines to support

Epiflow implementation with different cell types and markers. However, we strongly advise the reader to consult the available literature for optimal spectral flow cytometry experimental design and downstream analysis (den Braanker et al., 2021; Ferrer-Font et al., 2021; Fox et al., 2020; Park et al., 2020; T et al., 2021).

1. The guidelines for assigning fluorochromes to the antigen of interest used for traditional flow cytometry still apply to spectral flow cytometry. Match brighter fluorochromes with lowly expressed antigens. Co-expressed antigens should be assigned colors that have distinct spectra with low spread. If possible, consider using fluorochromes with high spillover spread or emitting in the autofluorescent channels (~500 nm) for positive events that get removed, like the viability stain.

2. Panel design can be supported using www.FluoroFinder.com. Ideally, build a panel with a low complexity index. This readout indicates how noisy the data will be given how similar the fluorochrome spectra are to each other.

3. Although not discussed in this protocol, it is critical to titrate each antibody on the target cell type before running the final panel to ensure that the signal is within range. This is also true for new antibody lots and clones. The histone antibodies were not originally titrated for this protocol as the signal was in range of the detectors and responded as expected in the various epigenetic drug validation experiments.

4. Utilizing isotype controls is a debated topic in this field (Andersen et al., 2016; Keeney et al., 1998). We did not use isotype controls in this work because we previously titrated most of our antibodies, which confirmed that the assay was sensitive and specific (Fig. S2, S3, S8).

5. Autofluorescent spectral signatures will be unique to each cell type and can change depending on factors related to cell stress and metabolism.

6. To ensure statistical power, capture at least 5,000 bead events and 10,000 cell events.

7. Unmixing controls vary depending on the sample. It's important to compare unmixing results using beads and cells before selecting the most appropriate option. For further details, please refer to Ferrer-Font et al. 2021.

8. Several factors can contribute to variability in spectral flow assays.

   a. Sample preparation: Inconsistent cell counts, temperature control, inadequate mixing, and improper storage conditions.

   b. Bead preparation: To generate spectra that are comparable, beads and cells must be treated identically. Any differences in processing or staining sequences can lead to beads binding antibodies differently than cells, producing spectral signatures that may not accurately represent the cell populations.

   c. Aurora daily quality control (QC): Calibration of the Aurora is essential after startup to ensure optimal performance. Before acquiring data, confirm that the Daily QC check has passed. This ensures that

258 optical alignment, laser delays, scaling factors, gain settings, and performance drift are optimized to
259 account for daily instrument variability.

260 9. Excessive dead cells and debris can arise from rough handling before viability staining, missed wash
261 steps, or from introducing bubbles during pipetting in 96-well plates. To minimize cell shearing, handle live
262 cells gently and avoid pipetting volumes exceeding 100 μL in 96-well plates to prevent introducing air.
263 Additionally, perform all wash steps as outlined in the protocol to ensure thorough washing (Protocols S1
264 and S2).

265 10. Cross-contamination of spectral signatures between neighboring wells can happen due to slow plate
266 decanting. To avoid this, decant quickly and swiftly (≤1 second) to ensure pellets remain at the well base
267 and prevent droplets from migrating to adjacent wells.

268 11. Excessive doublet populations can result from inadequate mixing during pellet resuspension or
269 prolonged storage at 4 °C. To address this, consider passing cells through a 0.45 μm filter and improving
270 sample mixing by setting the pipette to a larger volume setting of ~70-80 μL. Also, try mixing samples
271 immediately before analysis and avoid overnight storage of methanol-treated cells to prevent stickiness.

272

Materials and methods

The SCTi003-A (RRID:CVCL_C1W7) and WTC11 (UCSFi001-A, RRID:CVCL_Y803) control hiPSC lines were used throughout this study. KMT2D loss-of-function (LOF) hiPSC line was generated through CRISPR/Cas9 editing of exon 2 in the *KMT2D* gene. This resulted in a homozygous 2 bp deletion in the wildtype WTC11 iPSC line, creating the isogenic KMT2D-LOF model (KMT2D10.4). Room temperature refers to 22 °C. All hiPSC lines were karyotyped and confirmed to be free of mycoplasma. This protocol can be applied to samples run on traditional flow cytometers, including the Stratedigm S1000EXi benchtop flow cytometer. For this, the panel design process should be repeated to ensure that the fluorochromes selected are compatible with the instrument. Details on the Stratedigm assays are in Table S2. All experiments were conducted as n=3 biological triplicates. ChatGPT4o (AI) was used to assist in text refinement and code optimization.

Cell culture

hiPSCs were grown on 6-well plates (Corning) coated with 2D Matrigel (Corning) in mTeSR Plus media (Stem Cell Technologies) supplemented with Primocin (InvivoGen). Once the cells were ~70% confluent, the media was replaced with STEMdiff SMADi Neural Induction media (Stem Cell Technologies) supplemented with Primocin. The neural induction was performed following the manufacturer's protocol. Cells were subcultured at 70% confluency to maintain continuous mitosis events by day 7. All cultures were incubated at 37°C in a 5% CO2 incubator with daily media changes.

Drug Treatments

NPCs were cultured to 70% confluency and treated with three different concentrations of Trichostatin A (TSA; 0.5μM, 1μM, 10μM) or A485 (1μM, 10μM, 20μM). SCTi-003A, WTC11 and KMT2D10.4 hiPSCs were also grown to 70% confluency and treated with TSA (0.5μM, 1μM, 2μM), Vorinostat (SAHA; 0.5μM, 0.75μM,1μM), OICR-9429 (10μM, 20μM, 50μM) or CPI-455 HCl (10μM, 20μM, 50μM). Cells were treated for 4 hours with either the drug or DMSO, then harvested and processed according to the flow cytometry protocols outlined above.

Sample preparation

On day 7 NPCs were gently detached and resuspended in a round bottom 96-well plate. Cell pellets were stained with fixable viability dye (BD) for 15 minutes on a rotating platform at room temperature. Cells were then fixed in 4% PFA (Thermo Fisher) for 20 minutes at room temperature. For permeabilization, cells were incubated with 100% ice-cold methanol (Fisher Chemical) for 15 minutes in a -20°C freezer. For blocking, cells were incubated with 5% BSA for 30 minutes on a rotating platform at room temperature. Cells were then incubated with the appropriate antibody cocktail for 1 hour on a rotating platform at room temperature. Finally, cells were stained with FxCycle Flow Ready (Invitrogen) for 30 minutes on a rotating platform at room temperature. FxCycle was not removed from the solution prior to running on the cytometer. All incubations were performed with a shaking speed of ~80 rpm. Between each step (except FxCycle), cells were washed once in FACs buffer (0.5% BSA, Sigma-Aldrich). All centrifugal spins were performed at 4°C

309 for 5 minutes. Following the spin, a quick and swift decanting movement was used to ensure that sample
310 loss and cross-contamination were prevented. Single color controls (SCCs) were prepared using beads
311 (Invitrogen) or cells. Cells were used for all dye-based staining. After dyes and antibodies were added, the
312 samples were protected from light using foil.

313 **Spectral flow cytometry assay**

314 Data was acquired on a 5L Cytek Aurora analyzer (Cytek Biosciences). Before acquiring the data, ensure
315 that each sample is well-mixed by pipetting immediately before running the assay. Ensure that the Aurora
316 completed the warmup/start-up initialization and passed the quality control check. Run the spectral flow
317 cytometry assay according to user-defined settings. We utilized the following acquisition settings for NPCs:
318 Events to record: 10,000,000, Stopping time (sec): 10,000, Stopping volume (μL): 150, Flow rate: High,
319 FSC: 40, SSC: 20.

320 **Data unmixing**

321 Acquired data was unmixed with SpectroFlo v2 (Cytek Biosciences) without autofluorescence removal.
322 Unstained cells and SCCs (beads or cells) were used as references for unmixing, as detailed in Table S1.
323 After unmixing, both SCCs and fully stained samples were manually inspected for potential unmixing
324 artifacts in NxN plots (File S2) following recommended guidelines for spectral flow cytometry panel
325 optimization (Ferrer-Font et al., 2021).

326 **Gating, clustering and dimensionality reduction**

327 The data analysis workflow for gating and dimensionality reduction was built using the cloud-based OMIQ
328 analysis platform (File S3). To ensure all events were properly scaled, each feature was transformed using
329 arcsinh (File S3). Three gating strategies were implemented to optimize signal separation, exclude artifacts
330 or debris, and identify distinct cell populations, ensuring accurate downstream analysis.

331 *Event rate and cell quality gating:* First, time gating was applied to select events recorded with a stable
332 flow rate. This was followed by additional gating to isolate singlets, exclude debris, and discriminate live
333 and dead cells. Subsequent gating and analyses were performed within the live cell population.

334 *Manual gating as a benchmark:* This strategy involved the identification of apoptotic cells (cleaved
335 Caspase-3 positive cells), neuronal progenitor cells (PAX6 positive cells), and determining cell cycle status
336 (G0/G1-G2: FxCycle; mitosis: pH3-S10 positive cells). To account for differences in fluorescence intensity
337 signal observed in H3K9ac, H3K4me3, H3K14ac, and H3K27ac features, distinct gates were applied
338 targeting events with low, medium, and high fluorescence intensity within each cell cycle phase. Changes
339 in global H3 were assessed across G0/G1, G2, and mitosis. Fluctuations in H3-PTM fluorescence intensity,
340 potentially driven by H3 replication-dependent biogenesis (Armstrong and Spencer, 2021), were evaluated
341 by applying specific gates for each histone mark within the Total H3 gate (Fig. S7). After manual gating, the
342 subset of fully stained files was retained and the maximum number of live cells was randomly subsampled
343 from each replicate.

Unsupervised clustering and gating: Unsupervised clustering was performed using FlowSOM (Van Gassen et al., 2015). The resulting elbow meta-clusters ("fsom clusters"), representing distinct groupings of data that share similar characteristics, were embedded as gates for further analysis and comparison with manual gating. Dimensionality reduction was performed using optimized T-distributed stochastic neighbor embedding (opt-SNE) (Belkina et al., 2019). Data was exported from OMIQ and is available in the GitHub repository associated with this article. Please refer to File S3 for a detailed workflow, including feature selection, analysis parameters, and random seed details for each algorithm.

Data exploration and visualization

The data exploration and visualization workflow was built in R using the renv package (Renv v1.0.7), which creates reproducible R environments and ensures data analysis reproducibility. This workflow provides a graphical representation of the main features contributing to each FlowSOM cluster. Methods and statistical analyses are described in the figure legends. A comprehensive analysis and data visualization code, including input data, data processing steps, and visualization rationale, is available at [https://github.com/SerranoLab/Golden_etal_2024].

Reagents

Reagent	Company	Catalog number
mTeSR Plus	Stem Cell Technologies	100-0276
Primocin antimicrobial 1,000x stock	InvivoGen	ant-pm-1
Matrigel hESC-qualified matrix	Corning	354277
DPBS no calcium, no magnesium	Gibco	14190144
Accutase	Stem Cell Technologies	07920
STEMdiff SMADi Neural Induction Medium	Stem Cell Technologies	05839
UltraComp eBeads plus compensation beads	Invitrogen	01-3333-42
BD Horizon Fixable Viability 780	BD Biosciences	565388
BSA	Sigma-Aldrich	A9418
Paraformaldehyde 16% w/v aq. soln., methanol free	Thermo Fisher Scientific	043368.9M
Methanol	Fisher Chemical	A454-1
Acetyl-histone H3 (Lys9) (C5B11) Pacific Blue conjugate	Cell Signaling Technology	11857S
BD Horizon BV 650 anti-active caspase-3	BD Biosciences	570179
Acetyl-histone H3 (Lys14) (D4B9) Alexa Fluor 488 conjugate	Cell Signaling Technology	26828S
Phospho-histone H3 (Ser10) (D2C8) XP (Alexa Fluor 532 conjugate)	Cell Signaling Technology	52725S
Mono-methyl-histone H3 (Lys4) (D1A9) XP (PE conjugate)	Cell Signaling Technology	55800S
Acetyl-histone H3 (Lys27) (D5E4) XP (PE-Cy7 conjugate)	Cell Signaling Technology	30342S

Tri-methyl-histone H3 (Lys4) (C42D8) (Alexa Fluor 647 conjugate)	Cell Signaling Technology	12064S
Histone H3 (D1H2) XP (Alexa Fluor 700 conjugate)	Cell Signaling Technology	54826S
FxCycle Violet Ready Flow reagent	Invitrogen	R37166
PAX6 mFluor Violet 500 SE	Novus Biologicals	NBP2-47915MFV500
PAX6 PE (O18-1330)	BD Biosciences	561552
Trichostatin A	Cell Signaling Technologies	9950S
A485	Tocris	6387
Vorinostat	Cell Signaling Technologies	12520
OICR-9429	Selleckchem	S7833
CPI-455 HCL	Selleckchem	S8287

Acknowledgments

The authors would like to thank Dr. Shari Brezinsky for instrumental support, Irena Feng for supporting initial method optimization, and Sandeep Sreerama and Sandra Sulser for sample processing support. We thank Dr. Effie Apostolou for helpful discussions and revisions of the project.

This work was supported by the Center for Regenerative Medicine and Boston University Chobanian & Avedisian School of Medicine through start-up funds to M.A.S. This work was also supported by the Flow Cytometry Core Facility at Boston University. hiPSC lines WTC11 and KMT2D10.4 were provided by grant UM1 HL098160 to HJY from the National Heart, Lung, and Blood Institute.

Competing Interests

The authors declare no competing interests.

Data and resource availability

Data analysis code and details of R packages used are available at [https://github.com/SerranoLab/Golden_etal_2024]. Raw flow cytometry and unmixed spectral flow cytometry data will be made available in FlowRepository.

References

Andersen, M.N., Al-Karradi, S.N.H., Kragstrup, T.W., Hokland, M., 2016. Elimination of erroneous results in flow cytometry caused by antibody binding to Fc receptors on human monocytes and macrophages. Cytometry Pt A 89, 1001–1009. https://doi.org/10.1002/cyto.a.22995

Armenta-Castro, E., Reyes-Vallejo, T., Máximo-Sánchez, D., Herrera-Camacho, I., López-López, G., Reyes-Carmona, S., Conde-Rodríguez, I., Ramírez-Díaz, I., Aguilar-Lemarroy, A., Jave-Suárez, L.F., Milflores-Flores, L., Santos-Lopez, G., Reyes-Leyva, J., Vallejo-Ruiz, V., 2020. Histone H3K9 and H3K14 acetylation at the promoter of the LGALS9 gene is associated with mRNA levels in cervical cancer cells. FEBS Open Bio 10, 2305–2315. https://doi.org/10.1002/2211-5463.12973

Armstrong, C., Spencer, S.L., 2021. Replication-dependent histone biosynthesis is coupled to cell-cycle commitment. Proceedings of the National Academy of Sciences 118, e2100178118. https://doi.org/10.1073/pnas.2100178118

Belkina, A.C., Ciccolella, C.O., Anno, R., Halpert, R., Spidlen, J., Snyder-Cappione, J.E., 2019. Automated optimized parameters for T-distributed stochastic neighbor embedding improve visualization and analysis of large datasets. Nat Commun 10, 5415. https://doi.org/10.1038/s41467-019-13055-y

Bergamasco, M.I., Vanyai, H.K., Garnham, A.L., Geoghegan, N.D., Vogel, A.P., Eccles, S., Rogers, K.L., Smyth, G.K., Blewitt, M.E., Hannan, A.J., Thomas, T., Voss, A.K., 2024. Increasing histone acetylation improves sociability and restores learning and memory in *KAT6B*-haploinsufficient mice. J Clin Invest 134. https://doi.org/10.1172/JCI167672

Bui, H.-T., Wakayama, S., Kishigami, S., Park, K.-K., Kim, J.-H., Thuan, N.V., Wakayama, T., 2010. Effect of Trichostatin A on Chromatin Remodeling, Histone Modifications, DNA Replication, and Transcriptional Activity in Cloned Mouse Embryos1. Biology of Reproduction 83, 454–463. https://doi.org/10.1095/biolreprod.109.083337

Calder, A., Roth-Albin, I., Bhatia, S., Pilquil, C., Lee, J.H., Bhatia, M., Levadoux-Martin, M., McNicol, J., Russell, J., Collins, T., Draper, J.S., 2013. Lengthened G1 Phase Indicates Differentiation Status in Human Embryonic Stem Cells. Stem Cells and Development 22, 279–295. https://doi.org/10.1089/scd.2012.0168

Chari, T., Pachter, L., 2023. The specious art of single-cell genomics. PLOS Computational Biology 19, e1011288. https://doi.org/10.1371/journal.pcbi.1011288

Coronado, D., Godet, M., Bourillot, P.-Y., Tapponnier, Y., Bernat, A., Petit, M., Afanassieff, M., Markossian, S., Malashicheva, A., Iacone, R., Anastassiadis, K., Savatier, P., 2013. A short G1 phase is an intrinsic determinant of naïve embryonic stem cell pluripotency. Stem Cell Research 10, 118–131. https://doi.org/10.1016/j.scr.2012.10.004

Crump, N.T., Hazzalin, C.A., Bowers, E.M., Alani, R.M., Cole, P.A., Mahadevan, L.C., 2011. Dynamic acetylation of all lysine-4 trimethylated histone H3 is evolutionarily conserved and mediated by p300/CBP. Proceedings of the National Academy of Sciences 108, 7814–7819. https://doi.org/10.1073/pnas.1100099108

den Braanker, H., Bongenaar, M., Lubberts, E., 2021. How to Prepare Spectral Flow Cytometry Datasets for High Dimensional Data Analysis: A Practical Workflow. Front. Immunol. 12. https://doi.org/10.3389/fimmu.2021.768113

Ferrer-Font, L., Small, S.J., Lewer, B., Pilkington, K.R., Johnston, L.K., Park, L.M., Lannigan, J., Jaimes, M.C., Price, K.M., 2021. Panel Optimization for High-Dimensional Immunophenotyping Assays Using Full-Spectrum Flow Cytometry. Current Protocols 1, e222. https://doi.org/10.1002/cpz1.222

Fox, A., Dutt, T.S., Karger, B., Obregón-Henao, A., Anderson, G.B., Henao-Tamayo, M., 2020. Acquisition of High-Quality Spectral Flow Cytometry Data. Current Protocols in Cytometry 93, e74. https://doi.org/10.1002/cpcy.74

Golden, C., Williams, S., Serrano, M., 2024. Nuclear Histone 3 Post-Translational Modification Profiling in Whole Cells using Spectral Flow Cytometry [GitHub Repository]. URL https://github.com/SerranoLab/Golden_etal_2024.

Grebien, F., Vedadi, M., Getlik, M., Giambruno, R., Grover, A., Avellino, R., Skucha, A., Vittori, S., Kuznetsova, E., Smil, D., Barsyte-Lovejoy, D., Li, F., Poda, G., Schapira, M., Wu, H., Dong, A., Senisterra, G., Stukalov, A., Huber, K.V.M., Schönegger, A., Marcellus, R., Bilban, M., Bock, C., Brown, P.J., Zuber, J., Bennett, K.L., Al-awar, R., Delwel, R., Nerlov, C., Arrowsmith, C.H., Superti-Furga, G., 2015. Pharmacological targeting of the Wdr5-MLL interaction in C/EBPα N-terminal leukemia. Nat Chem Biol 11, 571–578. https://doi.org/10.1038/nchembio.1859

Grigoryev, S.A., Bulynko, Y.A., Popova, E.Y., 2006. The end adjusts the means: Heterochromatin remodelling during terminal cell differentiation. Chromosome Res 14, 53–69. https://doi.org/10.1007/s10577-005-1021-6

Hansen, K.H., Bracken, A.P., Pasini, D., Dietrich, N., Gehani, S.S., Monrad, A., Rappsilber, J., Lerdrup, M., Helin, K., 2008. A model for transmission of the H3K27me3 epigenetic mark. Nat Cell Biol 10, 1291–1300. https://doi.org/10.1038/ncb1787

Herzenberg, Leonore A., Tung, J., Moore, W.A., Herzenberg, Leonard A., Parks, D.R., 2006. Interpreting flow cytometry data: a guide for the perplexed. Nat Immunol 7, 681–685. https://doi.org/10.1038/ni0706-681

Karmodiya, K., Krebs, A.R., Oulad-Abdelghani, M., Kimura, H., Tora, L., 2012. H3K9 and H3K14 acetylation co-occur at many gene regulatory elements, while H3K14ac marks a subset of inactive inducible promoters in mouse embryonic stem cells. BMC Genomics 13, 424. https://doi.org/10.1186/1471-2164-13-424

Keeney, M., Gratama, J.W., Chin-Yee, I.H., Sutherland, D.R., 1998. Isotype controls in the analysis of lymphocytes and CD34+ stem and progenitor cells by flow cytometry--time to let go! Cytometry 34, 280–283.

Krejčí, J., Uhlířová, R., Galiová, G., Kozubek, S., Šmigová, J., Bártová, E., 2009. Genome-wide reduction in H3K9 acetylation during human embryonic stem cell differentiation. Journal of Cellular Physiology 219, 677–687. https://doi.org/10.1002/jcp.21714

Kubo, N., Chen, P.B., Hu, R., Ye, Z., Sasaki, H., Ren, B., 2024. H3K4me1 facilitates promoter-enhancer interactions and gene activation during embryonic stem cell differentiation. Molecular Cell 84, 1742-1752.e5. https://doi.org/10.1016/j.molcel.2024.02.030

Kueh, A.J., Bergamasco, M.I., Quaglieri, A., Phipson, B., Li-Wai-Suen, C.S.N., Lönnstedt, I.M., Hu, Y., Feng, Z.-P., Woodruff, C., May, R.E., Wilcox, S., Garnham, A.L., Snyder, M.P., Smyth, G.K., Speed, T.P., Thomas, T., Voss, A.K., 2023. Stem cell plasticity, acetylation of H3K14, and *de novo* gene activation rely on KAT7. Cell Reports 42, 111980. https://doi.org/10.1016/j.celrep.2022.111980

Larson, J.L., Yuan, G.-C., 2012. Chromatin States Accurately Classify Cell Differentiation Stages. PLOS ONE 7, e31414. https://doi.org/10.1371/journal.pone.0031414

Lasko, L.M., Jakob, C.G., Edalji, R.P., Qiu, W., Montgomery, D., Digiammarino, E.L., Hansen, T.M., Risi, R.M., Frey, R., Manaves, V., Shaw, B., Algire, M., Hessler, P., Lam, L.T., Uziel, T., Faivre, E., Ferguson, D., Buchanan, F.G., Martin, R.L., Torrent, M., Chiang, G.G., Karukurichi, K., Langston, J.W., Weinert, B.T., Choudhary, C., de Vries, P., Kluge, A.F., Patane, M.A., Van Drie, J.H., Wang, C., McElligott, D., Kesicki, E., Marmorstein, R., Sun, C., Cole, P.A., Rosenberg, S.H., Michaelides, M.R., Lai, A., Bromberg, K.D., 2017. Discovery of a selective catalytic p300/CBP inhibitor that targets lineage-specific tumours. Nature 550, 128–132. https://doi.org/10.1038/nature24028

Lauberth, S.M., Nakayama, T., Wu, X., Ferris, A.L., Tang, Z., Hughes, S.H., Roeder, R.G., 2013. H3K4me3 Interactions with TAF3 Regulate Preinitiation Complex Assembly and Selective Gene Activation. Cell 152, 1021–1036. https://doi.org/10.1016/j.cell.2013.01.052

Lee, M.G., Wynder, C., Bochar, D.A., Hakimi, M.-A., Cooch, N., Shiekhattar, R., 2006. Functional Interplay between Histone Demethylase and Deacetylase Enzymes. Molecular and Cellular Biology 26, 6395–6402. https://doi.org/10.1128/MCB.00723-06

Li, D.W., Yang, Q., Chen, J.T., Zhou, H., Liu, R.M., Huang, X.T., 2005. Dynamic distribution of Ser-10 phosphorylated histone H3 in cytoplasm of MCF-7 and CHO cells during mitosis. Cell Res 15, 120–126. https://doi.org/10.1038/sj.cr.7290276

Liu, X., Guo, C., Leng, T., Fan, Z., Mai, J., Chen, J., Xu, J., Li, Q., Jiang, B., Sai, K., Yang, W., Gu, J., Wang, J., Sun, S., Chen, Z., Zhong, Y., Liang, X., Chen, C., Cai, J., Lin, Y., Liang, J., Hu, J., Yan, G., Zhu, W., Yin, W., 2023. Differential regulation of H3K9/H3K14 acetylation by small molecules drives neuron-fate-induction of glioma cell. Cell Death Dis 14, 1–14. https://doi.org/10.1038/s41419-023-05611-8

Liu, Yin, Chen, S., Wang, S., Soares, F., Fischer, M., Meng, F., Du, Z., Lin, C., Meyer, C., DeCaprio, J.A., Brown, M., Liu, X.S., He, H.H., 2017. Transcriptional landscape of the human cell cycle. Proceedings of the National Academy of Sciences 114, 3473–3478. https://doi.org/10.1073/pnas.1617636114

Liu, Yiyuan, Pelham-Webb, B., Di Giammartino, D.C., Li, J., Kim, D., Kita, K., Saiz, N., Garg, V., Doane, A., Giannakakou, P., Hadjantonakis, A.-K., Elemento, O., Apostolou, E., 2017. Widespread Mitotic

Bookmarking by Histone Marks and Transcription Factors in Pluripotent Stem Cells. Cell Reports 19, 1283–1293. https://doi.org/10.1016/j.celrep.2017.04.067

Lo, W.-S., Trievel, R.C., Rojas, J.R., Duggan, L., Hsu, J.-Y., Allis, C.D., Marmorstein, R., Berger, S.L., 2000. Phosphorylation of Serine 10 in Histone H3 Is Functionally Linked In Vitro and In Vivo to Gcn5-Mediated Acetylation at Lysine 14. Molecular Cell 5, 917–926. https://doi.org/10.1016/S1097-2765(00)80257-9

Ma, Y., Kanakousaki, K., Buttitta, L., 2015. How the cell cycle impacts chromatin architecture and influences cell fate. Front. Genet. 6. https://doi.org/10.3389/fgene.2015.00019

Novo, D., 2022. A comparison of spectral unmixing to conventional compensation for the calculation of fluorochrome abundances from flow cytometric data. Cytometry Pt A 101, 885–891. https://doi.org/10.1002/cyto.a.24669

Park, J., Lee, K., Kim, K., Yi, S.-J., 2022. The role of histone modifications: from neurodevelopment to neurodiseases. Sig Transduct Target Ther 7, 1–23. https://doi.org/10.1038/s41392-022-01078-9

Park, L.M., Lannigan, J., Jaimes, M.C., 2020. OMIP-069: Forty-Color Full Spectrum Flow Cytometry Panel for Deep Immunophenotyping of Major Cell Subsets in Human Peripheral Blood. Cytometry Part A 97, 1044–1051. https://doi.org/10.1002/cyto.a.24213

Pelham-Webb, B., Polyzos, A., Wojenski, L., Kloetgen, A., Li, J., Di Giammartino, D.C., Sakellaropoulos, T., Tsirigos, A., Core, L., Apostolou, E., 2021. H3K27ac bookmarking promotes rapid post-mitotic activation of the pluripotent stem cell program without impacting 3D chromatin reorganization. Molecular Cell 81, 1732-1748.e8. https://doi.org/10.1016/j.molcel.2021.02.032

Petruk, S., Sedkov, Y., Johnston, D.M., Hodgson, J.W., Black, K.L., Kovermann, S.K., Beck, S., Canaani, E., Brock, H.W., Mazo, A., 2012. TrxG and PcG Proteins but Not Methylated Histones Remain Associated with DNA through Replication. Cell 150, 922–933. https://doi.org/10.1016/j.cell.2012.06.046

Richon, V.M., Webb, Y., Merger, R., Sheppard, T., Jursic, B., Ngo, L., Civoli, F., Breslow, R., Rifkind, R.A., Marks, P.A., 1996. Second generation hybrid polar compounds are potent inducers of transformed cell differentiation. Proc Natl Acad Sci U S A 93, 5705–5708.

Roederer, M., Darzynkiewicz, Z., Parks, D.R., 2004. Guidelines for the presentation of flow cytometric data. Methods Cell Biol 75, 241–256. https://doi.org/10.1016/s0091-679x(04)75010-4

Ronzoni, S., Faretta, M., Ballarini, M., Pelicci, P., Minucci, S., 2005. New method to detect histone acetylation levels by flow cytometry. Cytometry Part A 66A, 52–61. https://doi.org/10.1002/cyto.a.20151

Seuter, S., Heikkinen, S., Carlberg, C., 2013. Chromatin acetylation at transcription start sites and vitamin D receptor binding regions relates to effects of 1α,25-dihydroxyvitamin D3 and histone deacetylase inhibitors on gene expression. Nucleic Acids Research 41, 110–124. https://doi.org/10.1093/nar/gks959

Sze, C.C., Cao, K., Collings, C.K., Marshall, S.A., Rendleman, E.J., Ozark, P.A., Chen, F.X., Morgan, M.A., Wang, L., Shilatifard, A., 2017. Histone H3K4 methylation-dependent and -independent functions of Set1A/COMPASS in embryonic stem cell self-renewal and differentiation. Genes Dev. 31, 1732–1737. https://doi.org/10.1101/gad.303768.117

T, L., Lm, W., Tm, A., N, S., M, P., S, V.G., F, M., 2021. An updated guide for the perplexed: cytometry in the high-dimensional era. Nature immunology 22. https://doi.org/10.1038/s41590-021-01006-z

Ushey, K., Wickham, H., 2024a. Introduction to renv [WWW Document]. URL https://rstudio.github.io/renv/articles/renv.html (accessed 9.30.24).

Ushey, K., Wickham, H., 2024b. rstudio/renv [WWW Document]. URL https://github.com/rstudio/renv, https://rstudio.github.io/renv/ (accessed 9.29.24).

Van Gassen, S., Callebaut, B., Van Helden, M.J., Lambrecht, B.N., Demeester, P., Dhaene, T., Saeys, Y., 2015. FlowSOM: Using self-organizing maps for visualization and interpretation of cytometry data. Cytometry Part A 87, 636–645. https://doi.org/10.1002/cyto.a.22625

Van Rechem, C., Ji, F., Chakraborty, D., Black, J.C., Sadreyev, R.I., Whetstine, J.R., 2021. Collective regulation of chromatin modifications predicts replication timing during cell cycle. Cell Reports 37, 109799. https://doi.org/10.1016/j.celrep.2021.109799

Vigushin, D.M., Ali, S., Pace, P.E., Mirsaidi, N., Ito, K., Adcock, I., Coombes, R.C., 2001. Trichostatin A Is a Histone Deacetylase Inhibitor with Potent Antitumor Activity against Breast Cancer in Vivo1. Clinical Cancer Research 7, 971–976.

543 Vinogradova, M., Gehling, V.S., Gustafson, A., Arora, S., Tindell, C.A., Wilson, C., Williamson, K.E., Guler,
544 G.D., Gangurde, P., Manieri, W., Busby, J., Flynn, E.M., Lan, F., Kim, H., Odate, S., Cochran, A.G.,
545 Liu, Y., Wongchenko, M., Yang, Y., Cheung, T.K., Maile, T.M., Lau, T., Costa, M., Hegde, G.V.,
546 Jackson, E., Pitti, R., Arnott, D., Bailey, C., Bellon, S., Cummings, R.T., Albrecht, B.K., Harmange,
547 J.-C., Kiefer, J.R., Trojer, P., Classon, M., 2016. An inhibitor of KDM5 demethylases reduces
548 survival of drug-tolerant cancer cells. Nat Chem Biol 12, 531–538.
549 https://doi.org/10.1038/nchembio.2085
550 Weng, M.K., Zimmer, B., Pöltl, D., Broeg, M.P., Ivanova, V., Gaspar, J.A., Sachinidis, A., Wüllner, U.,
551 Waldmann, T., Leist, M., 2012. Extensive Transcriptional Regulation of Chromatin Modifiers during
552 Human Neurodevelopment. PLOS ONE 7, e36708. https://doi.org/10.1371/journal.pone.0036708

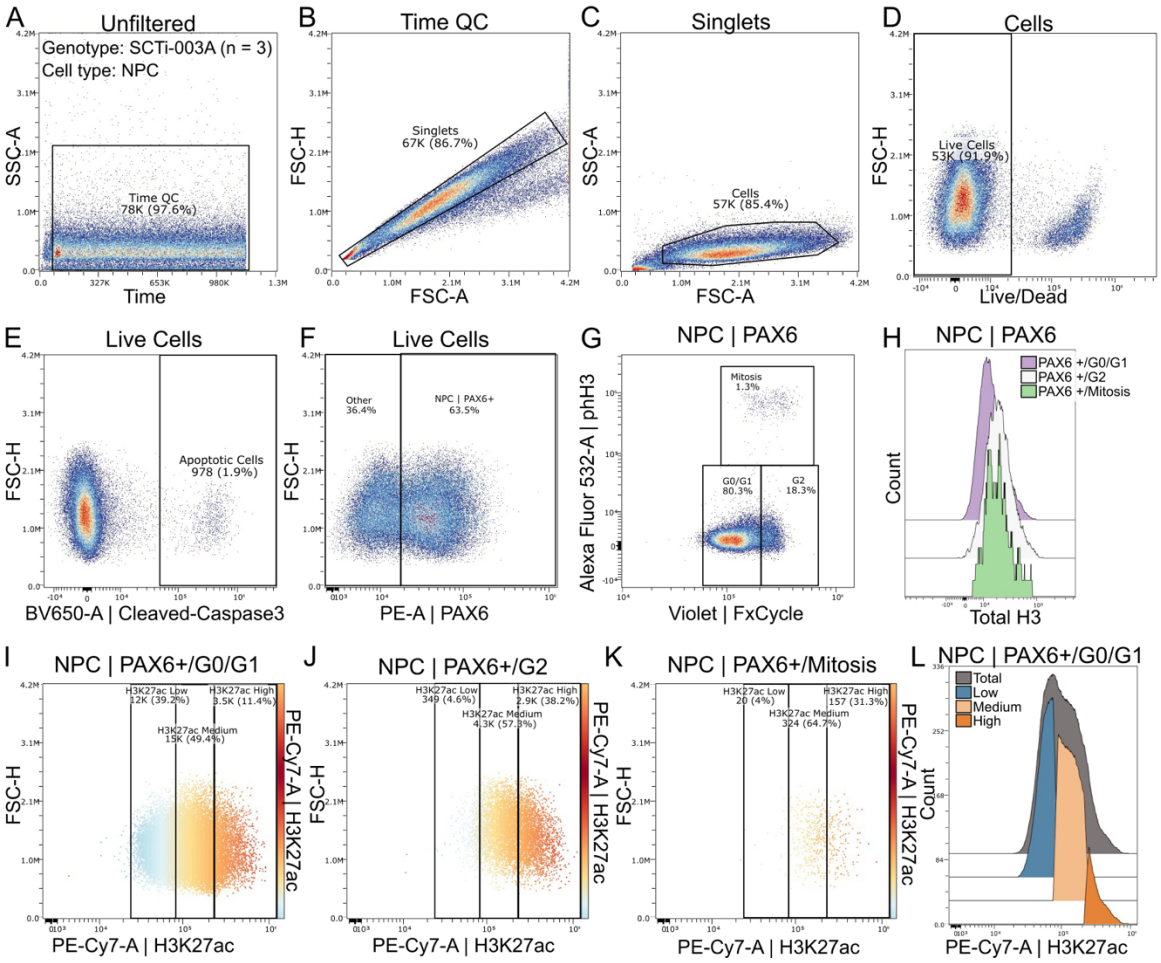

Figure 1. Scatter plots and histograms of manual gating strategies to select high quality events, identify neuronal progenitor cells, their cell cycle status, and histone H3-PTM fluorescence values. (A-D)**.** Cell quality gates to capture single cells recorded at a stable flow rate during acquisition. Subsampling and downstream analyses were performed using Live Cells gate. (E-L) Traditional two-dimensional gating strategy. (E) Within the live cells group, late apoptotic cells (cleaved-Caspase3 positive) are identified. (F) NPCs (PAX6 positive cells) were gated along with cells of low PAX6 expression ("Other"). (G) FxCycle and H3S10ph (pH3-S10) gates were used to identify NPCs in G0/G1, G2, and mitosis. (H) Histogram showing levels of total H3 at G0/G1, G2, and mitosis. Note comparable levels of total H3 during G2 and mitosis. (I-L) Gates to identify low, medium, and high fluorescence intensity values of H3K27ac in each cell cycle phase. Color-scale in panels I-K is used to aid more precise gating of H3 PTM features expected to be distributed as gradients rather than positive-negative cell populations. The same gating strategy was applied to all other H3-PTM assessed. Percent values (%) represent the events of a given gate present in root gate Live cells.

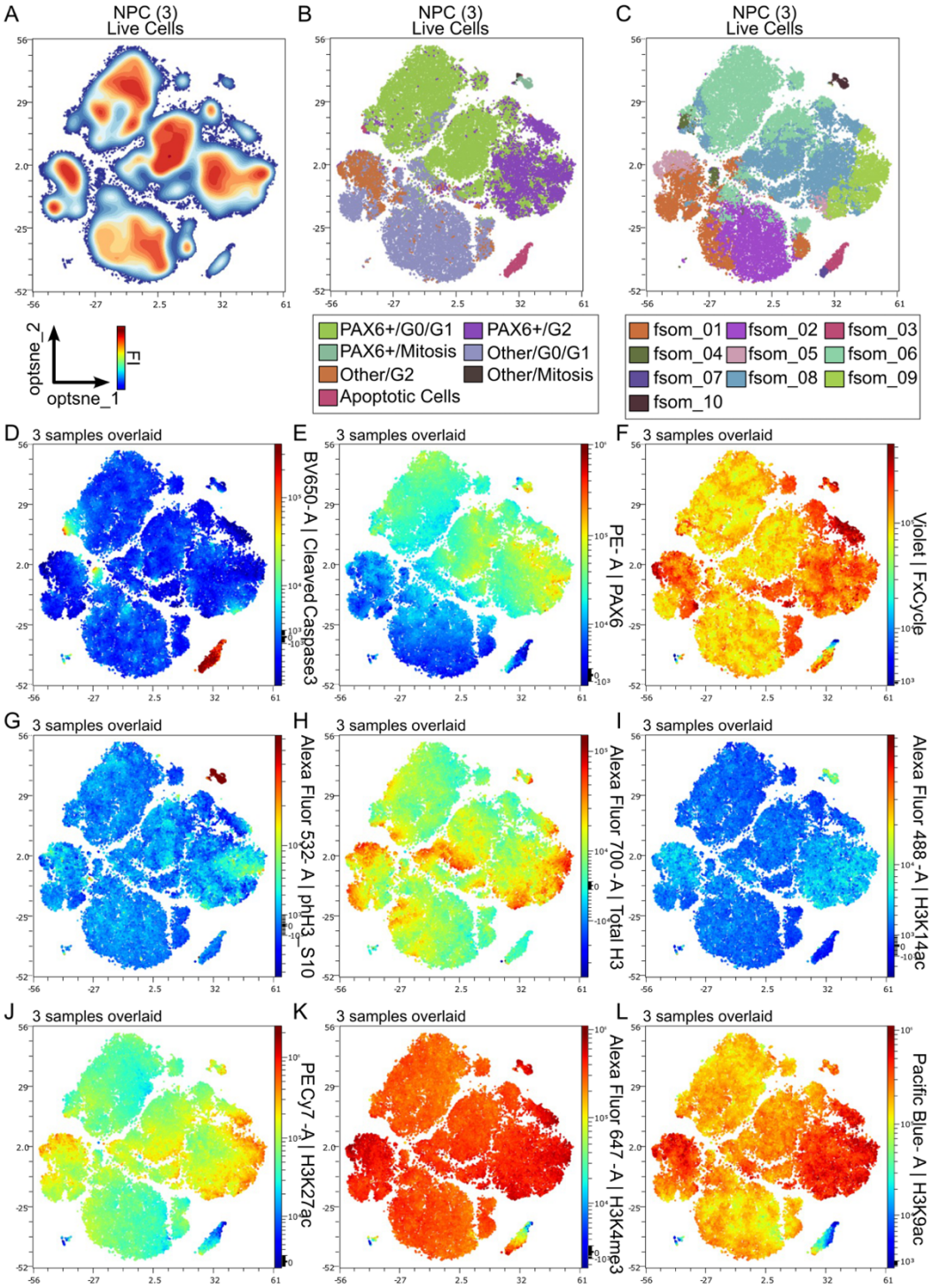

Figure 2. Visualization of manual gating and unsupervised clustering in opt-SNE two-dimensional space. (A) opt-SNE density plot of concatenated NPC samples (n = 3). (B) Cluster identification from traditional two-dimensional gating visualized in the opt-SNE dimensions. (C) Curated FlowSOM clusters visualized in the opt-SNE two-dimensional space. (D-L) Fluorescence intensity values of each feature plotted as a color-continuous scale in opt-SNE twp-dimensional space. The fluorescence intensity (FI) gradient for each feature shows blue for low intensity, green/yellow for medium intensity, and red for high intensity.

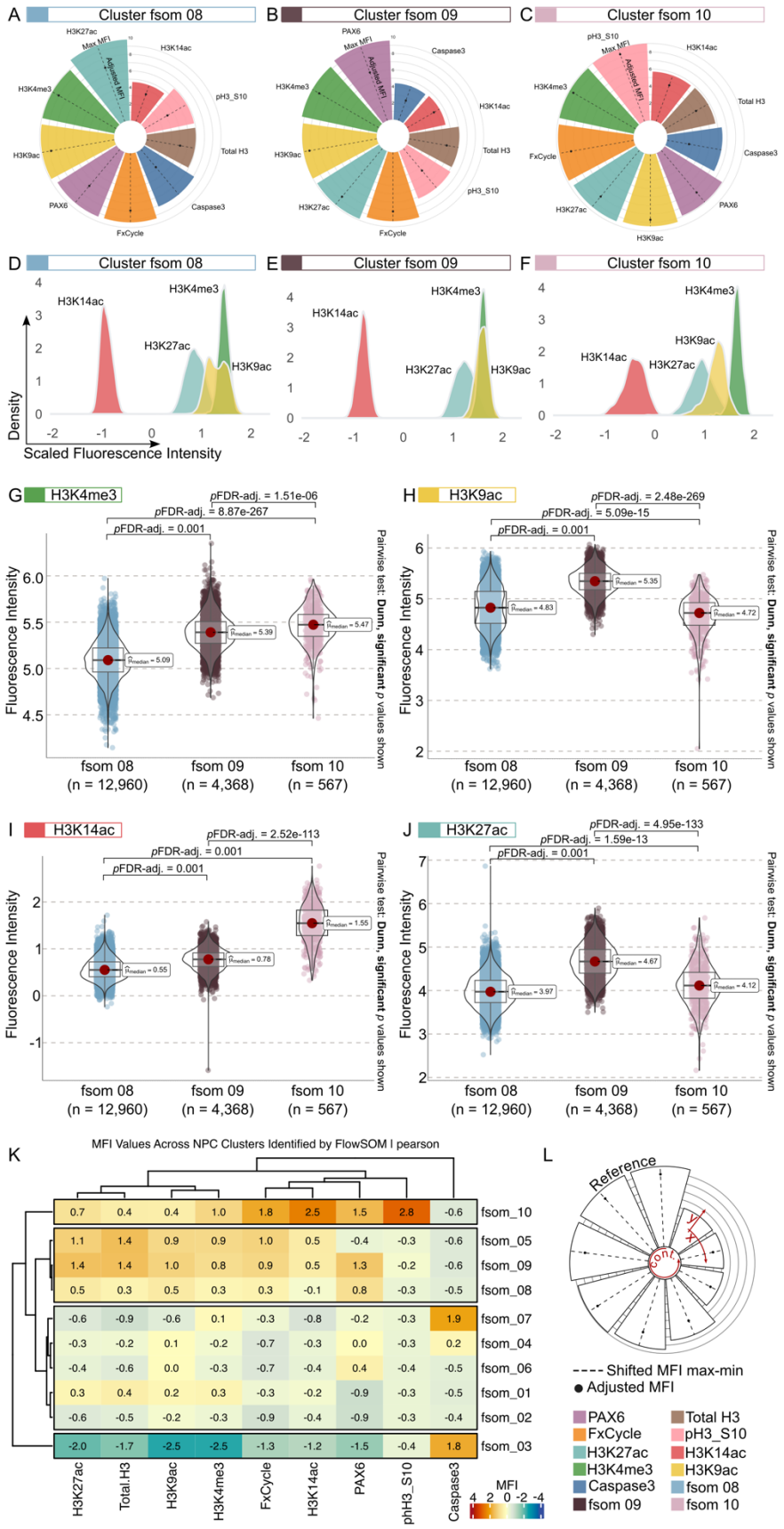
A
Cluster fsom 08
B
Cluster fsom 09
C
Cluster fsom 10
Max MFI
Adjusted MFI
H3K27ac
H3K14ac
pH3_S10
Total H3
Caspase3
PAX6
FxCycle
H3K9ac
H3K4me3
D
E
F
Density
Scaled Fluorescence Intensity
G
H3K4me3
pFDR-adj. = 1.51e-06
pFDR-adj. = 8.87e-267
pFDR-adj. = 0.001
H
H3K9ac
pFDR-adj. = 2.48e-269
pFDR-adj. = 5.09e-15
pFDR-adj. = 0.001
I
H3K14ac
pFDR-adj. = 2.52e-113
pFDR-adj. = 0.001
pFDR-adj. = 0.001
J
H3K27ac
pFDR-adj. = 4.95e-133
pFDR-adj. = 1.59e-13
pFDR-adj. = 0.001
Fluorescence Intensity
Pairwise test: Dunn, significant p values shown
fsom 08
(n = 12,960)
fsom 09
(n = 4,368)
fsom 10
(n = 567)
K
MFI Values Across NPC Clusters Identified by FlowSOM | pearson
fsom_10
fsom_05
fsom_09
fsom_08
fsom_07
fsom_04
fsom_06
fsom_01
fsom_02
fsom_03
H3K27ac
Total.H3
H3K9ac
H3K4me3
FxCycle
H3K14ac
PAX6
phH3_S10
Caspase3
MFI
L
Reference
Cont.
Shifted MFI max-min
Adjusted MFI
PAX6
Total H3
FxCycle
pH3_S10
H3K27ac
H3K14ac
H3K4me3
H3K9ac
Caspase3
fsom 08
fsom 09
fsom 10

Figure 3. High-dimensional exploration and assessment of H3-PTM profiles across clusters in NPCs. Data analysis and visualization strategies to evaluate feature contributions and distributions to each cluster and assess H3-PTM signatures. (A-C) Circular bar plots displaying the contribution of each feature in selected clusters. Median Fluorescence Intensity (MFI) values were transformed to ensure that all values were positive and greater than zero [MFI shifted = mfi + abs(min(mfi)) + 1]. Values were then summarized by feature (colored bars) within each cluster displaying maximum (outer end of the bar), minimum (inner end of the bar), and median values (shifted MFI, dot in the midline of each bar). Features (bars) are ordered from larger to smaller MFI values in a counterclockwise direction to highlight their contributions to each cluster. (D-F) Density plots showing H3-PTM scaled FI values and distributions in each cluster. (G-J) Violin plots of FI for H3K4me3 (G), H3K9ac (H), H3K14ac (I), and H3K27ac (J) across fsom_08, fsom_09, and fsom_10. Dunn pairwise test, statistically significant p-values shown. (K) Heatmap displaying the MFI values across 10 NPC clusters. To assess the correlation between H3-PTM, cell cycle status, and expression levels of PAX6, clustering of scaled MFI values (displayed within the heatmap) was

Figure S1: Validation of nuclear and membrane compartment staining in SCTi-003A hiPSCs.

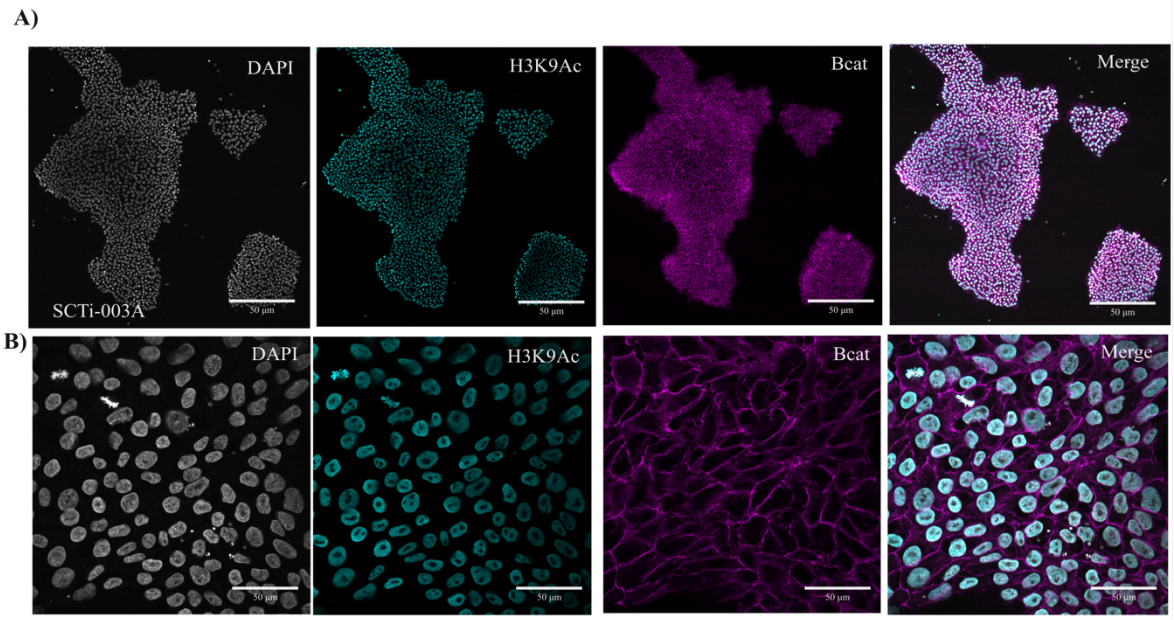

Figure S1: Immunofluorescent staining validation of cell membrane integrity and nuclear antigen localization. Confocal microscopy images of SCTi-003A hiPSCs. Cell colonies were fixed on glass coverslips and stained for β-catenin (Bcat) and histone 3 lysine 9 acetylation (H3K9ac) to assess membrane integrity and nuclear antigen location, respectively. (A) 10x magnification and (B) 63x magnification confocal images of SCTi-003A hiPSC colonies. Images were acquired on a Zeiss LSM 710 confocal microscope. Scale Bar: 50 μM.

Figure S2. Drug validation assay of hiPSC-derived NPCs using spectral flow cytometry protocol

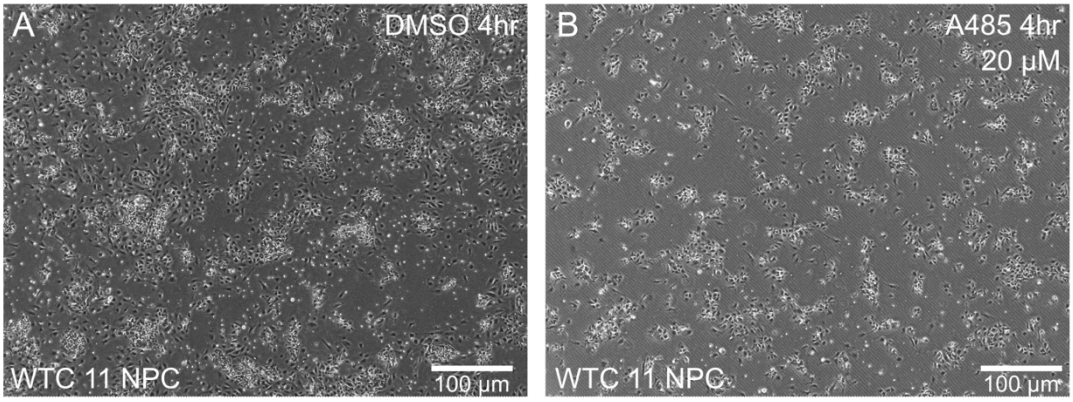

C EpiFlow Assessment of H3-PTM features after TSA and A-485 treatment.

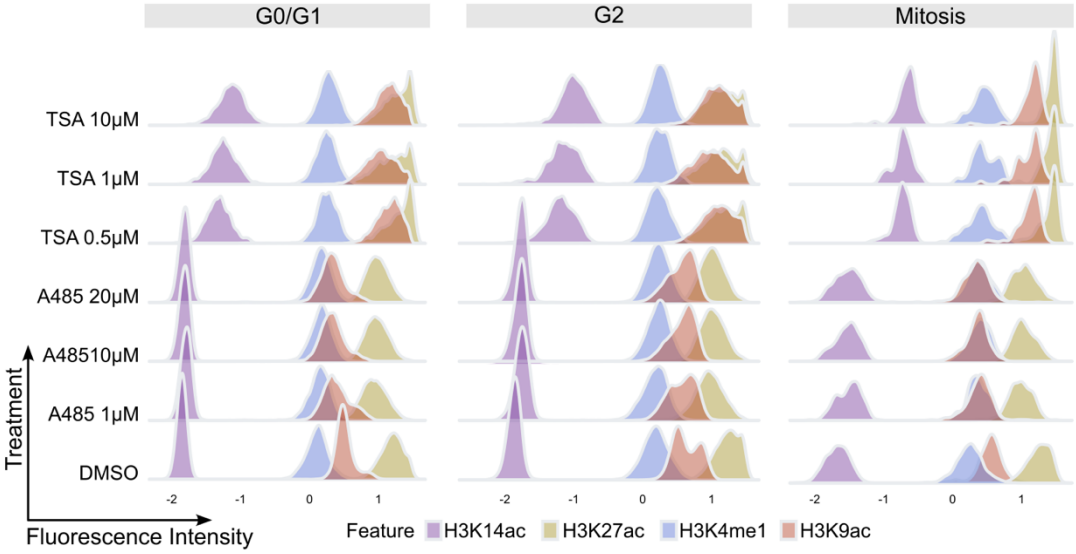

D

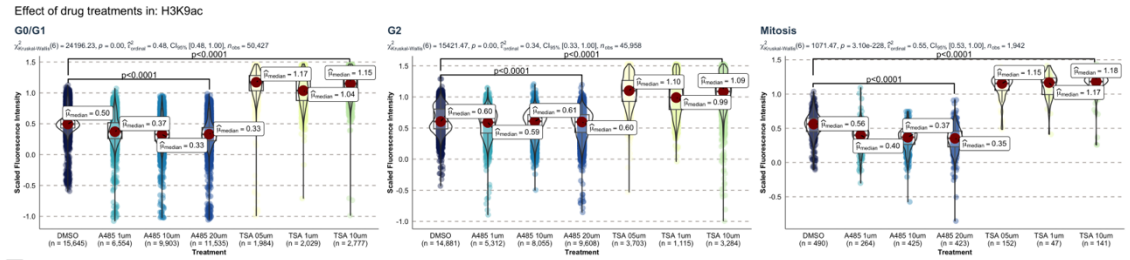

F

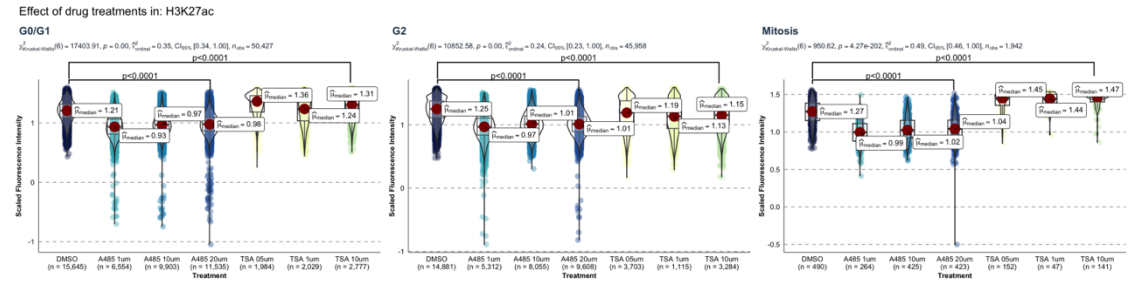

Figure S2. Validation of spectral flow cytometry protocol using selective epigenetic protein inhibitors. Spectral flow cytometry analysis of WTC11 NPC treated with TSA and A485. TSA is a histone deacetylase I/II inhibitor, resulting in increased histone acetylation. A485 is a histone acetyltransferase inhibitor that targets p300/CBP, resulting in decreased histone acetylation. For each drug treatment, cells were treated for 4 hours with DMSO (A), A485 (B), or TSA. A representative brightfield image from one concentration of A485 is shown. Superimposed density histogram plots for H3K9ac, H3K27ac, H3K4me1, and H3K14ac features across all drug concentrations display how the signal is distributed within each group throughout the cell cycle (C). Violin plots of the same groups confirm that the drugs were able to significantly alter H3-PTM acetylation levels (D, E). Replicates n=3 per group. Scale bar: 100 um. TSA: Trichostatin A. NPC: neural progenitor cells.

Figure S3. Drug validation assay of hiPSCs using conventional flow cytometry protocol

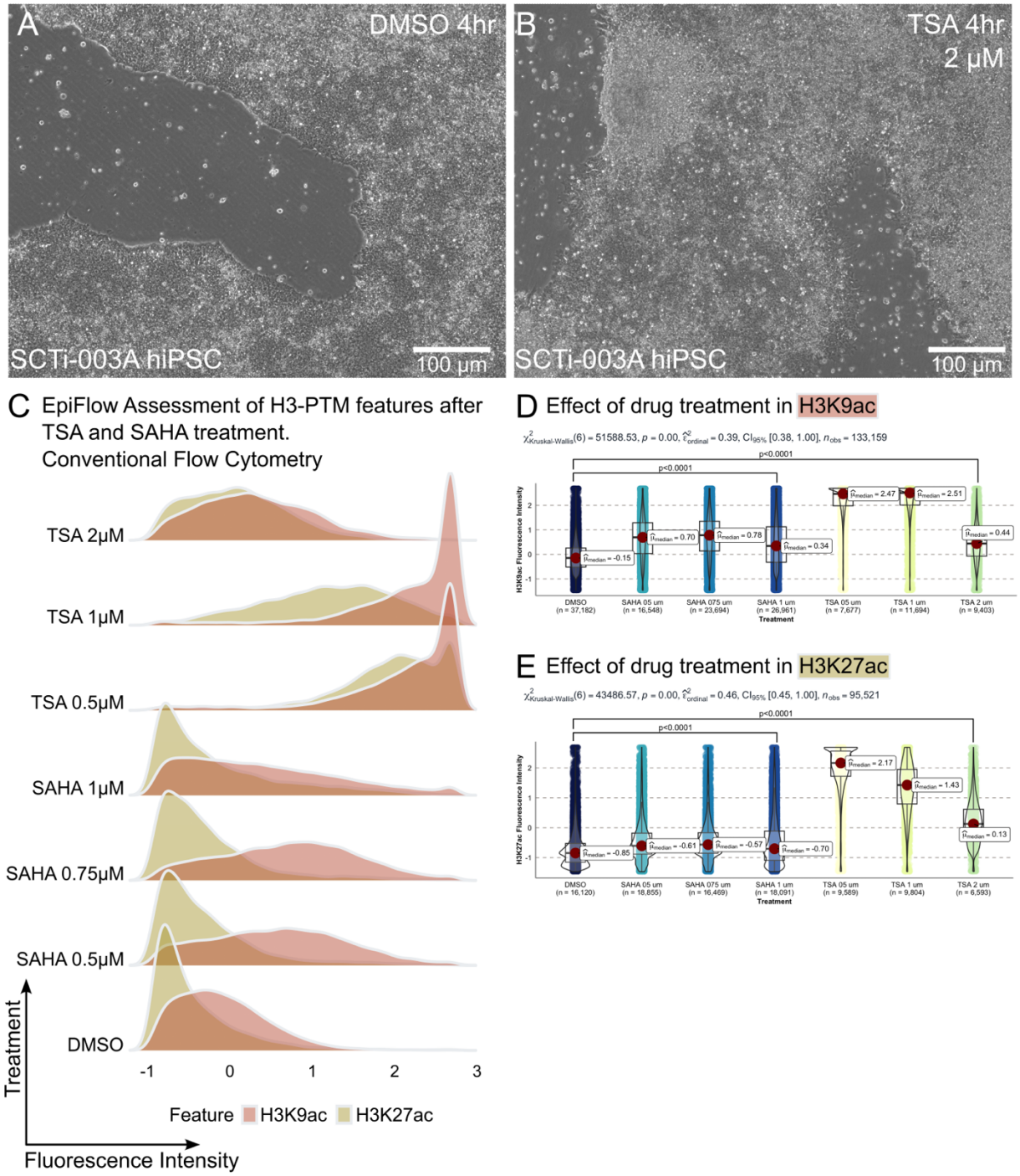

Figure S3. Validation of conventional flow cytometry protocol using epigenetic protein inhibitors. Conventional flow cytometry analysis of SCTi-003A hiPSCs treated with TSA and Vorinostat (SAHA). TSA and SAHA are histone deacetylase I/II inhibitors, resulting in increased histone acetylation. For each drug treatment, cells were treated for 4 hours with DMSO (A), TSA (B), or SAHA. A representative brightfield image from one concentration of SAHA is shown. Superimposed density histogram plots for H3K9ac and H3K27ac features across all drug concentrations show how the signal is distributed in each group (C). Violin

plots of the same groups confirm that the drugs were able to significantly alter H3-PTM acetylation levels (D, E). Replicates n=3 per group. Scale bar: 100 um. TSA: Trichostatin A. SAHA: Vorinostat. hiPSC: human induced pluripotent stem cells.

Figure S4. Drug validation assay targeting H3K4 methylation in hiPSCs using conventional flow cytometry

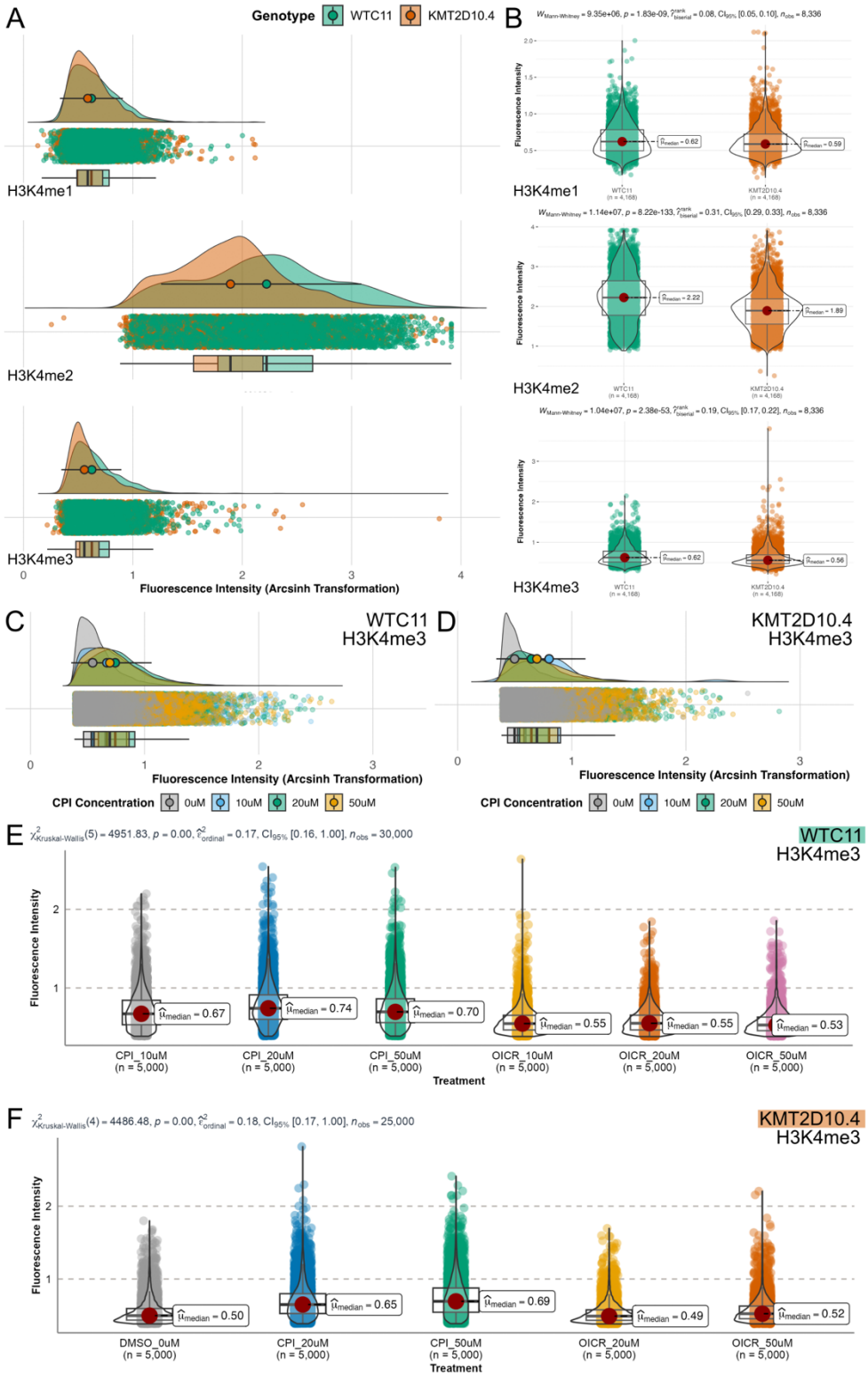

Figure S4. EpiFlow Detects Subtle Changes in H3K4 Methylation Marks. EpiFlow sensitivity was validated using a KMT2D loss-of-function (LOF) hiPSC line, which was generated through CRISPR/Cas9 editing of exon 2 in the KMT2D gene. This resulted in a homozygous 2 bp deletion in the wildtype WTC11 iPSC line, creating the KMT2D-LOF model (KMT2D10.4). WTC11 and KMT2D10.4 hiPSCs were incubated with DMSO or varying concentrations of OICR (H3K4me antagonist), or CPI (H3K4me agonist), for six days in culture. Data was acquired using conventional flow cytometry, preprocessed in OMIQ (scaling, gating, subsetting, subsampling), and analyzed in R. All plotted events correspond to H3K4 methylation within the H3-positive gate. (A-B) Rain plots (A) and violin plots (B) comparing fluorescence intensities of H3K4me1, H3K4me2, and H3K4me3 in KMT2D10.4 mutants versus WTC11. Statistically significant reductions in signal intensity and event counts are observed in the mutant line (Mann-Whitney U test, $p < 0.05$ for all marks). (C-D) H3K4me3 levels in WTC11 (C) and KMT2D10.4 (D) hiPSCs treated with CPI (10 μM, 20 μM, and 50 μM) and OICR (10 μM, 20 μM, and 50 μM). (E-F): Violin plots and statistical analysis of H3K4me3 levels in WTC11 (E) and KMT2D10.4 (F) after treatment with CPI and OICR (Kruskal-Wallis test, $p < 0.05$; 3 biological replicates).

Figure S5. Distribution of H3 PTM fluorescence intensity in NPCs across 10 FlowSOM clusters.

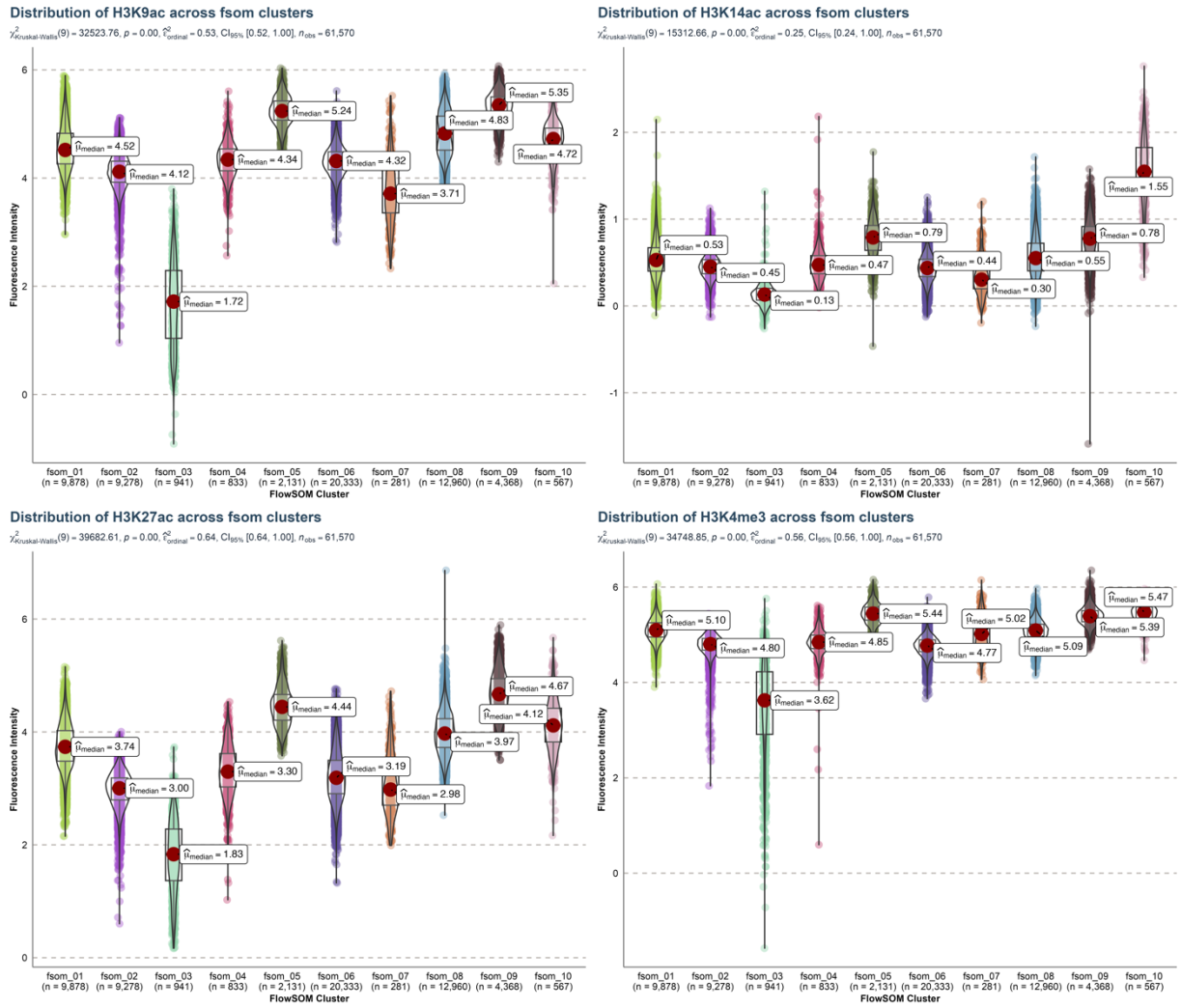

Figure S5. Distribution of H3 PTM fluorescence intensity in NPCs across 10 FlowSOM clusters. Violin plots of fluorescence intensity distributions for H3K9ac, H3K14ac, H3K27ac, and H3K4me3 across 10 clusters. Median values for each cluster are indicated with red dots, and their corresponding numerical values are labeled. Krustal-Wallis test shows significant differences in each feature assessed H3K9ac $\chi^2(9) = 32523.76$, $p<0.0001$; H3K14ac $\chi^2(9) = 15312.66$, $p<0.0001$; H3K27ac $\chi^2(9) = 39682.61$, $p<0.0001$; H3K4me3 $\chi^2(9) = 34748.85$, $p<0.0001$.

Figure S6. Assessment of H3 PTM signatures and cell cycle markers within clusters.

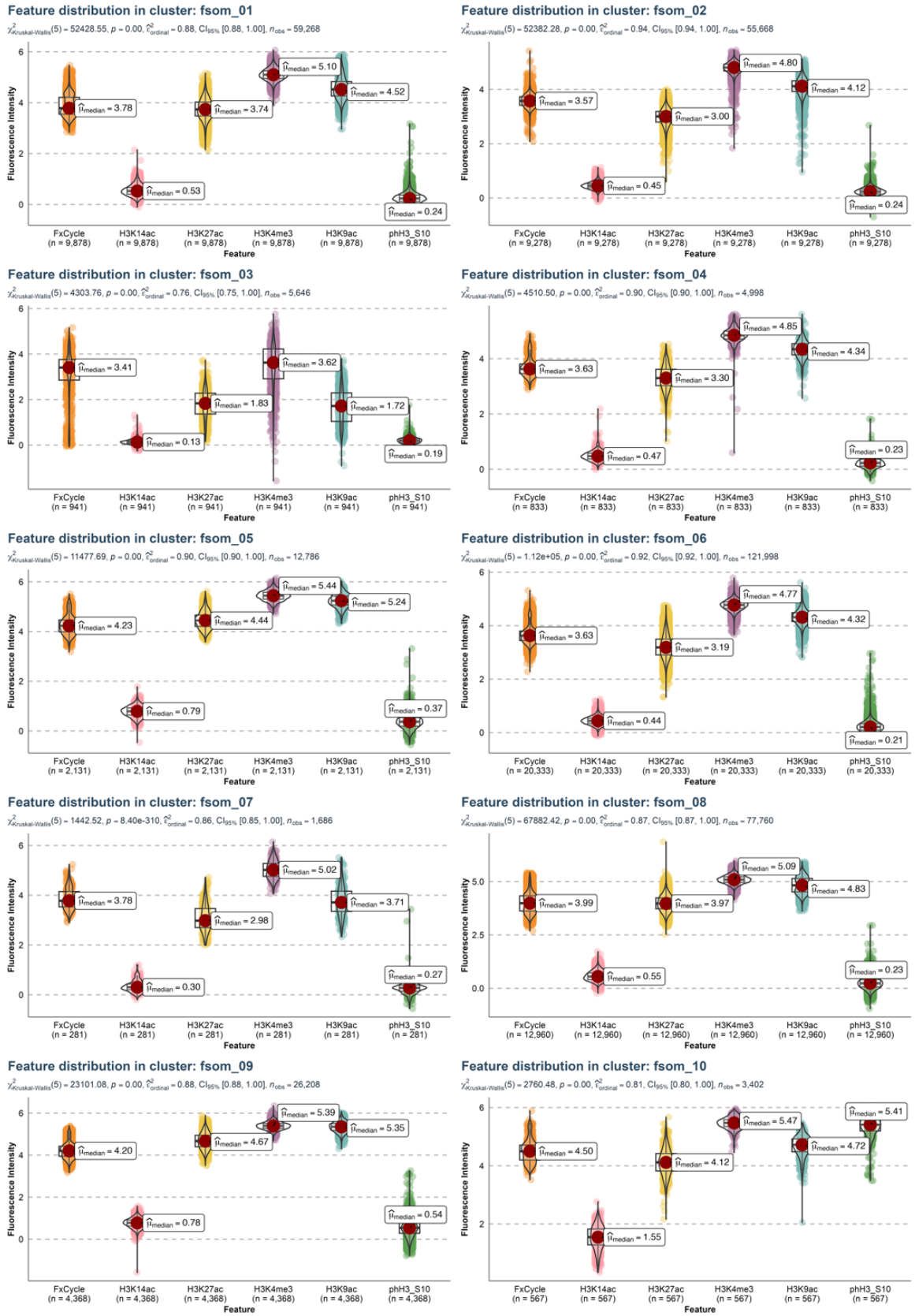

Figure S6. Assessment of H3 PTM signatures and cell cycle markers within clusters. Violin plots representing fluorescence intensity distributions of FxCycle, H3K14ac, H3K27ac, H3K4me3, H3K9ac, and phH3_S10 across 10 clusters (fsom_01 to fsom_10). Boxplots within each violin plot show the interquartile range and median fluorescence intensity values (red spot). Kruskal-Wallis test was applied to compare fluorescence intensities of all features within each cluster. Dunn's pairwise test was performed for post-hoc analysis. Sample sizes (n) are indicated for each feature in each cluster.

Figure S7. Comparison of Gating Strategies for H3 PTMs and Cell Cycle Markers Across G0/G1, G2, and Mitosis in NPCs.

Figure S7. Comparison of Gating Strategies for H3 PTMs and Cell Cycle Markers Across G0/G1, G2, and Mitosis in NPCs. Violin plots of all features across gated cell populations in different cell cycle phases. Kruskal-Wallis test statistics and p-values are provided for each feature. Dunn pairwise comparisons are available in GitHub Repository.

Figure S8. Titration experiment for specific reagents.

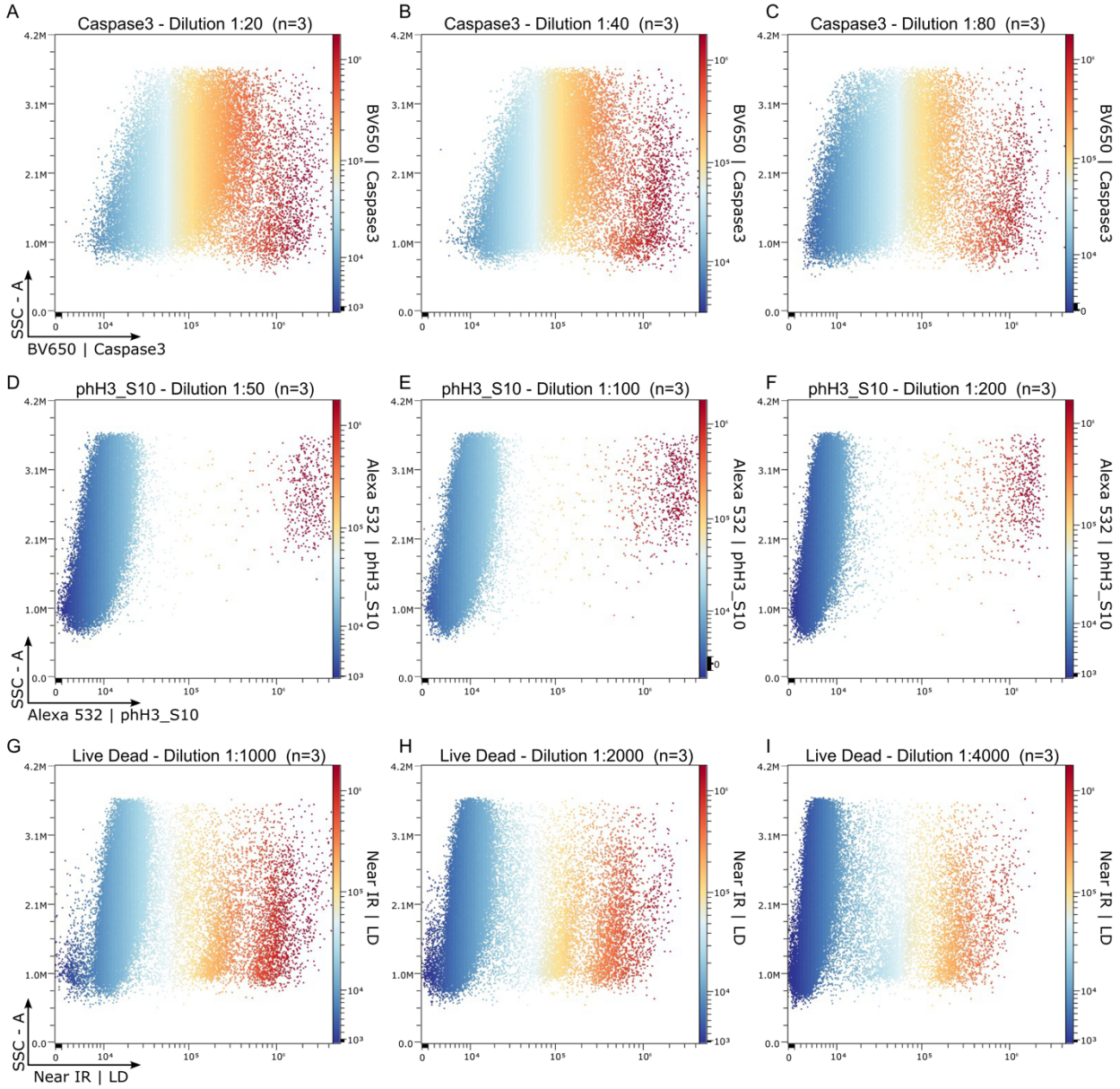

Figure S8. Titration experiment for specific reagents. A-C. Caspase3 antibody was titrated at 1:20, 1;40, and 1:80 dilutions. The 1:200 dilution was selected for experiments. D-F: Phospho-Histone H3 (Ser10) was titrated at 1:50, 1:100, and 1:200. A dilution of 1:400 was chosen for future experiments because the signal was still nearing the detection limits at the highest tested dilution. G-I. Live dead dye staining was titrated at 1:1,000, 1:2,000, and 1:4,000. Similar to phH3, a dilution of 1:8,000 for the Live/Dead stain was selected because the signal was still nearing the detection limits at the highest tested dilution.

Table S1. Spectral unmixing controls

Laser	Fluorochrome	Marker	Clone	Vendor	Catalog #	Unmixing
355	Violet	FxCycle/DNA	NA	Thermo Fisher	R37166	Cells
405	Pacific Blue	H3K9ac	C5B11	Cell Signaling	11857S	Beads
405	BV650	Active Caspase-3	C92-605.rMAb	BD	570179	Beads
405	mFluorViolet 500 SE	PAX6[(1)]	PAX6/1166	Novus Biologicals	47915MFV500	Beads
488	Alexa Fluor 488	H3K14ac	D4B9	Cell Signaling	26828	Beads
488	Alexa Fluor 532	PhosphoH3 (Ser10)	D2C8	Cell Signaling	52725	Beads
561	PE	PAX6[(2)]	O18-1330	BD	561552	Beads
561	PE	H3K4me1[(1)]	D1A9	Cell Signaling	55800S	Beads
561	PE-Cy7	H3K27ac	D5E4	Cell Signaling	30342	Beads
640	Alexa Fluor 647	H3K4me3[(2)]	C42D8	Cell Signaling	12064	Beads
640	Alexa Fluor 700	Total H3	D1H2	Cell Signaling	54826	Beads
640	Near IR 780	Fixable Viability	NA	BD	565388	Cells

[(1)] Included in the panel for drug treatment validation assay **(Figure S2)**

[(2)] Excluded in the panel for drug treatment validation assay **(Figure S2)**

Reagents

- Acetyl-Histone H3 (Lys9) (Cell Signaling Technologies, catalog number: 28036S)
- Acetyl-Histone H3 (Lys27) (Cell Signaling Technologies, catalog number: 15562S)
- Histone H3 647 (Cell Signaling Technologies, catalog number: 12230S)
- Mono-Methyl-Histone H3 (Lys4) (Cell Signaling Technologies, catalog number: 55800S)
- Di-Methyl-Histone H3 (Lys4) (Cell Signaling Technologies, catalog number: 31777S)
- Tri-Methyl-Histone H3 (Lys4) (Cell Signaling Technologies, catalog number: 62255S)

Table S1: Stratedigm Antibody Panel

Antibody	Catalog Number	Dilution	Volume	FACs Buffer	Total volume
Acetyl-Histone H3 (Lys9)*	28036S	1:50	12 μL	588 μL	600 μL
Histone H3 647*	12230S	1:50	12 μL	588 μL	600 μL
Acetyl-Histone H3 (Lys27)*	15562S	1:50	12 μL	588 μL	600 μL
Mono-Methyl-Histone H3 (Lys4)*	55800S	1:50	12 μL	588 μL	600 μL
Di-Methyl-Histone H3 (Lys4)*	31777S	1:50	12 μL	588 μL	600 μL
Tri-Methyl-Histone H3 (Lys4)*	62255S	1:50	12 μL	588 μL	600 μL
Acetyl-Histone H3 (Lys9) **SCC**	28036S	1:50	6 μL	294 μL	300 μL
Acetyl-Histone H3 (Lys27) **SCC**	15562S	1:50	6 μL	294 μL	300 μL
Mono-Methyl-HistoneH3(Lys4)**SCC**	55800S	1:50	6 μL	294 μL	300 μL
Di-Methyl-Histone H3 (Lys4) **SCC**	31777S	1:50	6 μL	294 μL	300 μL
Tri-Methy-Histone (Lys4) **SCC**	62255S	1:50	6 μL	294 μL	300 μL
Histone H3 647 **SCC**	12230S	1:50	6 μL	294 μL	300 μL
Live/Dead **SCC**	L34963	n/a	n/a	n/a	n/a

* **Denotes that the antibody can be combined into their respective sample.**

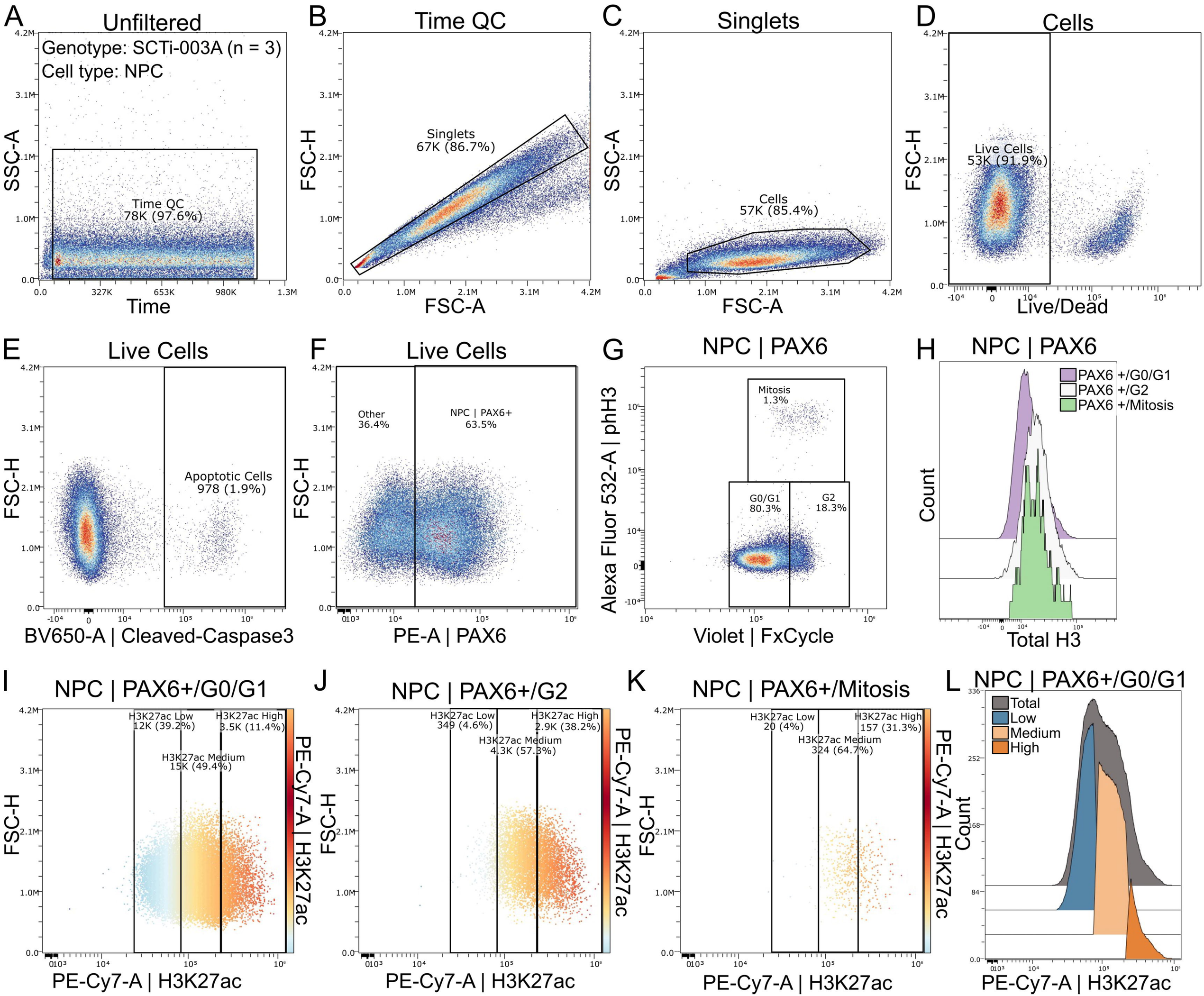
A
Unfiltered
Genotype: SCTi-003A (n = 3)
Cell type: NPC
Time QC
78K (97.6%)
SSC-A
Time
B
Time QC
Singlets
67K (86.7%)
FSC-H
FSC-A
C
Singlets
Cells
57K (85.4%)
SSC-A
FSC-A
D
Cells
Live Cells
53K (91.9%)
FSC-H
Live/Dead
E
Live Cells
Apoptotic Cells
978 (1.9%)
FSC-H
BV650-A | Cleaved-Caspase3
F
Live Cells
Other
36.4%
NPC | PAX6+
63.5%
FSC-H
PE-A | PAX6
G
NPC | PAX6
Mitosis
1.3%
G0/G1
80.3%
G2
18.3%
Alexa Fluor 532-A | phH3
Violet | FxCycle
H
NPC | PAX6
PAX6 +/G0/G1
PAX6 +/G2
PAX6 +/Mitosis
Count
Total H3
I
NPC | PAX6+/G0/G1
H3K27ac Low
12K (39.2%)
H3K27ac High
3.5K (11.4%)
H3K27ac Medium
15K (49.4%)
FSC-H
PE-Cy7-A | H3K27ac
PE-Cy7-A | H3K27ac
J
NPC | PAX6+/G2
H3K27ac Low
349 (4.6%)
H3K27ac High
2.9K (38.2%)
H3K27ac Medium
4.3K (57.3%)
FSC-H
PE-Cy7-A | H3K27ac
PE-Cy7-A | H3K27ac
K
NPC | PAX6+/Mitosis
H3K27ac Low
20 (4%)
H3K27ac High
157 (31.3%)
H3K27ac Medium
324 (64.7%)
FSC-H
PE-Cy7-A | H3K27ac
PE-Cy7-A | H3K27ac
L
NPC | PAX6+/G0/G1
Total
Low
Medium
High
Count
PE-Cy7-A | H3K27ac

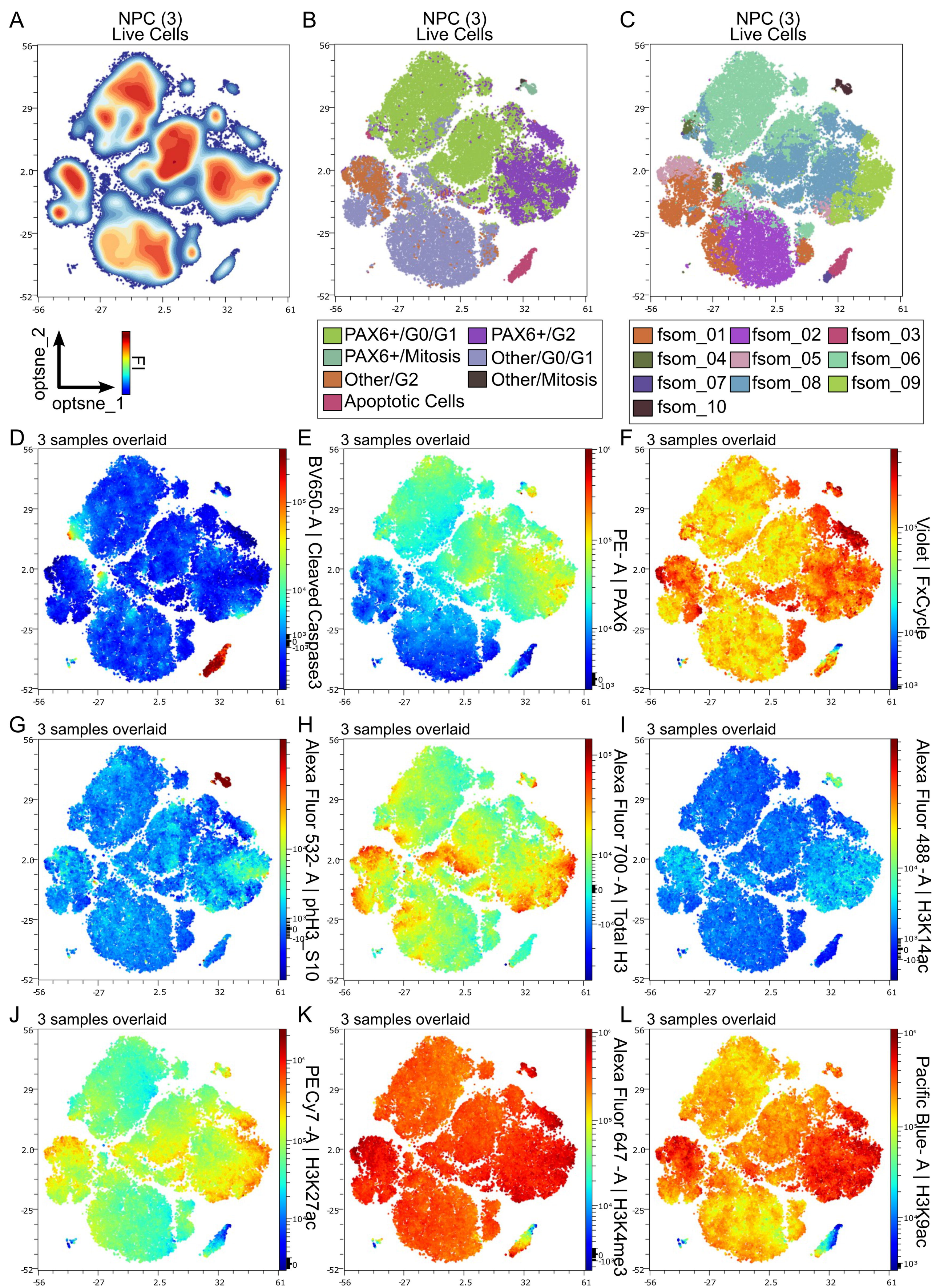
A
NPC (3)
Live Cells
B
NPC (3)
Live Cells
C
NPC (3)
Live Cells
optsne_2
optsne_1
FI
PAX6+/G0/G1
PAX6+/G2
PAX6+/Mitosis
Other/G0/G1
Other/G2
Other/Mitosis
Apoptotic Cells
fsom_01
fsom_02
fsom_03
fsom_04
fsom_05
fsom_06
fsom_07
fsom_08
fsom_09
fsom_10
D
3 samples overlaid
BV650-A | Cleaved Caspase3
E
3 samples overlaid
PE- A | PAX6
F
3 samples overlaid
Violet | FxCycle
G
3 samples overlaid
Alexa Fluor 532- A | phH3_S10
H
3 samples overlaid
Alexa Fluor 700 -A | Total H3
I
3 samples overlaid
Alexa Fluor 488 -A | H3K14ac
J
3 samples overlaid
PECy7 -A | H3K27ac
K
3 samples overlaid
Alexa Fluor 647 -A | H3K4me3
L
3 samples overlaid
Pacific Blue- A | H3K9ac

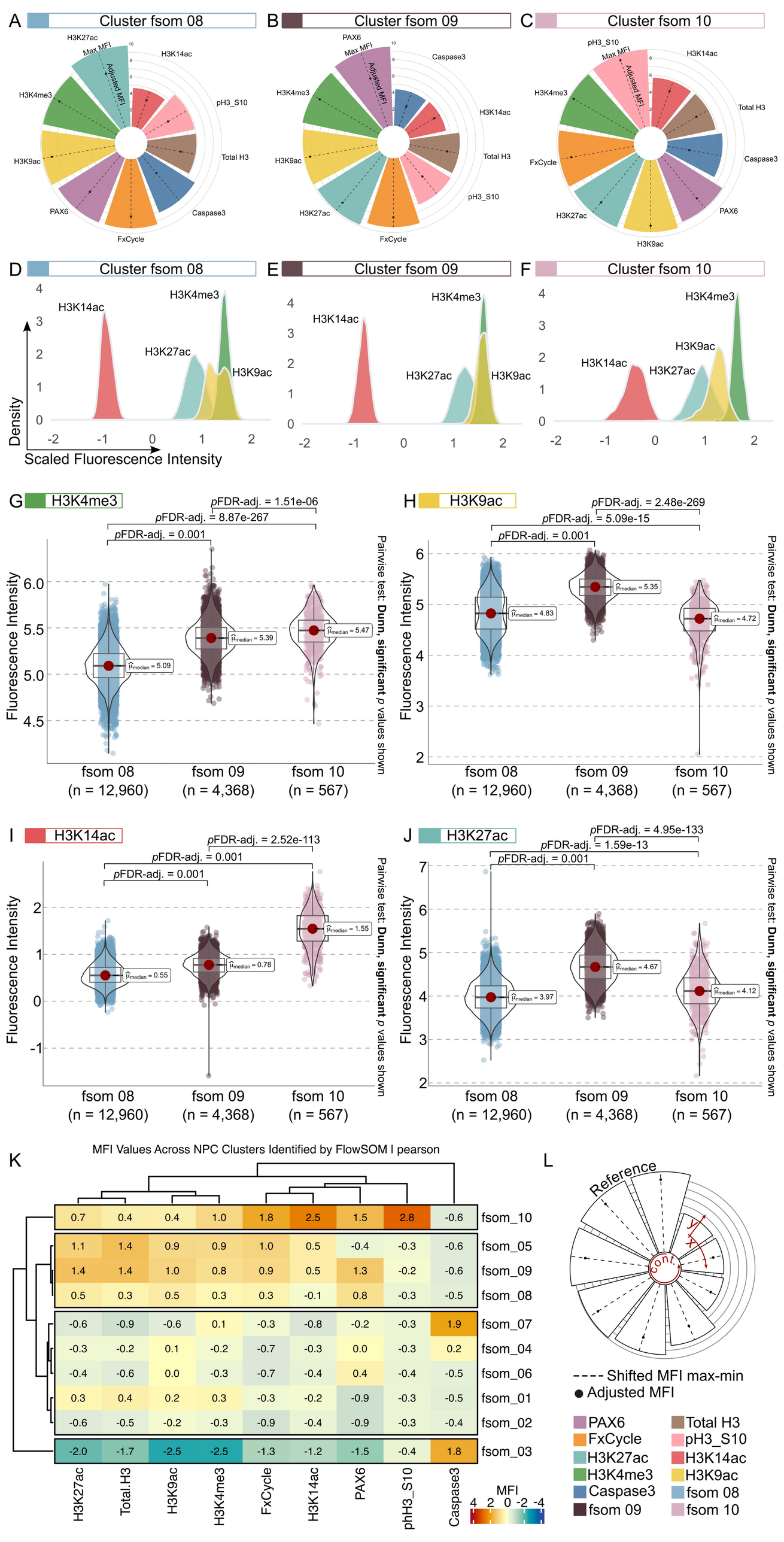
A
Cluster fsom 08
B
Cluster fsom 09
C
Cluster fsom 10
H3K27ac
Max MFI
Adjusted MFI
H3K14ac
pH3_S10
Total H3
Caspase3
FxCycle
PAX6
H3K9ac
H3K4me3
D
Cluster fsom 08
E
Cluster fsom 09
F
Cluster fsom 10
Density
Scaled Fluorescence Intensity
G
H3K4me3
pFDR-adj. = 1.51e-06
pFDR-adj. = 8.87e-267
pFDR-adj. = 0.001
Fluorescence Intensity
Pairwise test: Dunn, significant p values shown
fsom 08 (n = 12,960)
fsom 09 (n = 4,368)
fsom 10 (n = 567)
H
H3K9ac
pFDR-adj. = 2.48e-269
pFDR-adj. = 5.09e-15
pFDR-adj. = 0.001
I
H3K14ac
pFDR-adj. = 2.52e-113
pFDR-adj. = 0.001
pFDR-adj. = 0.001
J
H3K27ac
pFDR-adj. = 4.95e-133
pFDR-adj. = 1.59e-13
pFDR-adj. = 0.001
K
MFI Values Across NPC Clusters Identified by FlowSOM I pearson
fsom_10
fsom_05
fsom_09
fsom_08
fsom_07
fsom_04
fsom_06
fsom_01
fsom_02
fsom_03
H3K27ac
Total.H3
H3K9ac
H3K4me3
FxCycle
H3K14ac
PAX6
phH3_S10
Caspase3
MFI
L
Reference
cont.
Shifted MFI max-min
Adjusted MFI
PAX6
FxCycle
H3K27ac
H3K4me3
Caspase3
fsom 09
Total H3
pH3_S10
H3K14ac
H3K9ac
fsom 08
fsom 10